Identification of a stress-sensitive anorexigenic neurocircuit from medial prefrontal cortex to lateral hypothalamus in humans and mice

Rachel E Clarke[1], Katharina Voigt[2], Romana Stark[1], Urvi Bharania[1], Harry Dempsey[1], Alex Reichenbach[1], Sarah H Lockie[1], Mathieu Mequinion[1], Felicia Reed[1], Sasha Rawlinson[1], Juan Nunez-Iglesias[4], Claire J. Foldi[1], Alexxai V. Kravitz[3], Antonio Verdejo-Garcia[2], Zane B. Andrews[1]

1. Monash Biomedicine Discovery Institute and Department of Physiology, Monash University, Clayton, Victoria, 3800, Australia.
2. Turner Institute for Brain and Mental Health, Monash University, Clayton, Victoria, 3800, Australia
3. Departments of Psychiatry, Anesthesiology, and Neuroscience, Washington University in St Louis, St Louis, MO, US
4. Monash Biomedicine Discovery Institute and Department of Anatomy and Developmental Biology, Monash University, Clayton 3800, Victoria, Australia

Corresponding author:

Prof Z. B. Andrews: Email: Zane.Andrews@monash.edu Tel: +61 3 9905 8165

Disclosure Statement: The Authors have nothing to disclose

Abstract

Animal models that examine neural circuits controlling food intake often lack translational relevance. To address this limitation, we identified neural network dynamics related to homeostatic state and BMI in humans. This approach predicted a novel pathway projecting from the medial prefrontal cortex (mPFC) to the lateral hypothalamus (LH) in humans. We then dissected the mechanistic underpinnings of this human-relevant mPFC-LH circuit in mice. Chemogenetic or optogenetic activation of the mPFC-LH pathway in mice suppressed food intake and motivated sucrose-seeking. Fibre photometry demonstrated this pathway was active in response to acute stress or prior to novel environment or object exposure, suggesting a role in the predictive assessment of potential threat. Food consumption suppressed mPFC-LH neuronal activity, independent of metabolic state or palatability. Finally, inhibition of this circuit increased feeding and motivated behaviour under mild stress and chronic ablation caused weight gain. These studies identify the mPFC-LH as a novel stress-sensitive anorexigenic neural pathway involved in the cortical control of food intake and motivated reward-seeking.

Introduction

Body weight regulation is driven by neurobiological processes directed by genes implicated in the neuronal control of feeding [1, 2]. Significant advances have been made in recent decades using animal models that reveal the involvement of specific neural circuits controlling aspects of feeding, body weight control and energy balance, although these have largely centered on homeostatic systems governed by the hypothalamus and brain stem [3]. A modern environment poses a number of challenges for biological systems to regulate food intake and body weight, such as the need to encode and balance physiological interoceptive signals in combination with motivational and affective inputs, including reward and stress. In line with this, attention has now shifted to the higher-order cognitive and emotional processes that influence feeding behaviour, which are encoded by corticolimbic neural structures [4, 5]. What remains to be determined is how specific neurocircuits responsible for cognitive control of food intake override homeostatic signals to promote non-homeostatic food consumption and lead to dysregulation of body weight maintenance.

The medial prefrontal cortex (mPFC) is consistently identified as a key brain region implicated in the valuation of food [6, 7]. mPFC activity is associated with subjective health and taste ratings of food in self-reported dieters, and this activity varies based on whether an individual exerts dietary self-control or not [6]. In addition, mPFC activity is greater when individuals are asked to choose between healthy and unhealthy food options in a fasted state relative to a sated state [7], suggesting mPFC is sensitive to homeostatic information. Obese individuals consistently display stronger activation of the mPFC in response to images of food than healthy weight controls [8, 9, 10]. Moreover, when asked to choose between healthy and unhealthy food options in a fasted state, obese individuals display significantly stronger mPFC activation compared to their healthy-weight counterparts [7]. However, it is not possible to conclude that greater activity of the mPFC drives overconsumption of palatable food. For example, studies in patients with anorexia nervosa show similar elevated mPFC activity in response to images of foods compared to healthy controls [11]. Collectively, these studies show that it is difficult to accurately assign a function based on brain imaging of a single region, reinforcing the notion that diverse connectivity patterns must be examined [12]. Recent evidence from animal models suggests that communication between the hypothalamus and both cortical and subcortical structures is critical to influence appetite, reward and feeding behaviour [13, 14, 15, 16]. Consistent with this, human imaging studies demonstrate that the hypothalamus is functionally connected to a broad range of cortical and subcortical structures, including those involved in food valuation [17, 18]. However, functional connectivity assessed through fMRI does not directly represent anatomical connectivity or functionality, as a number of regions that are not connected still observe functional correlations [19].

In order to gain a translationally relevant and detailed understanding of how cortical and hypothalamic neural structures coordinate the regulation of food intake, functional imaging measures in humans need to be integrated with mechanistic insights that are only afforded by specific neural circuit manipulation in animal models. Here, we employed a reverse translational approach to first identify specific cortico-hypothalamic circuitry related to hunger and satiety in humans and then functionally manipulate these circuits in mouse models to examine their influence on food intake, motivation and behaviour. In this study, we performed resting-state fMRI and applied a novel neural network modelling approach to data collected across a wide BMI range under both hunger and sated conditions to explore how homoeostatic state affected dynamic connectivity between the cortex and hypothalamus. In humans, hunger was associated with reduced inhibitory signalling via a direct pathway from the mPFC to the lateral hypothalamus (LH). We then systematically examined the functional role of this mPFC-LH circuit in feeding and motivated behaviour in mice using chemogenetic, optogenetic and

fiber photometry approaches. Our results show that the mPFC-LH pathway responds to stress and food consumption and that activation of the circuit reduces motivation and feeding, whereas inhibition increases food consumption. Thus, we identify a previously uncharacterized stress-sensitive neural pathway that suppresses food intake and motivation and regulates body weight.

Methods – Human Studies

Participants

Fifty-thee participants (29 females, mean age = 24.70, SD = 6.33) were recruited from the general community. Participants' BMI ranged from 18 to 38kg/m^2: 30 had healthy weight (18-24.9kg/m^2), 9 were overweight (BMI = 25-30 kg/m^2) and 14 were obese (BMI > 30 kg/m^2). An initial screening interview assured that these participants (1) had no history of hypertension or diabetes, (2) had no neurological and psychiatric illness, or (3) were not on psychoactive medication affecting cognitive functioning or cerebral blood flow. All participants were naive to the purpose of the study, gave written consent before participating, and were reimbursed with $100 gift card vouchers. The Monash University Human Research Ethics Committee approved the study (2019-5979-30222) following the Declaration of Helsinki. All data and codes are now available on the Open Science Framework (DOI 10.17605/OSF.IO/CFRSH) : https://osf.io/cfrsh/.

Experimental procedure and MRI data acquisition

Participants completed two resting-state fMRI scans, one after an overnight fast (hunger condition) and one after a standardised breakfast (satiety condition). In both conditions, participants were instructed to have a typical meal (700-1000kj) between 7.30pm and 8.30pm on the night prior to their scan refrain from eating or drinking (except for water) until their morning scan. For the satiety condition, participants received a standard breakfast (293 kcal) one hour prior to their scan. Subjective self-reports of hunger (1 = not hungry at all; 7 = very hungry) revealed a significant difference in the perception of hunger between hunger (M = 4.63; SD = 1.46) and satiety (M = 3.12; SD = 1.58) condition ($t(52) = 4.73$, $p < 0.001$). All scans were scheduled in the morning between 9am and 10am and on average there were 5.82 days apart (SD = 3.73 days). Scheduling the participant's first scan as either part of the hunger or satiety condition was counterbalanced across participants. For a detailed description of iamge acquisition, data analysis and Spectral Dynamic Causal Modeling (spDCM) of network function, see supplemental methods and materials.

Methods – Animal Studies

All experiments were conducted in accordance with the Monash Animal Ethics Committee guidelines. C57BL/6 male mice were obtained from the Monash Animal Services facility. Vglut1-ires-cre male mice on a C57BL/6 background were obtained from the Jackson Laboratory (B6.Slc17a7-IRES2-Cre-D; stock number 023527) and bred in the Monash Animal Services Facility. All mice were aged between 8-10 weeks at beginning of experiments. Mice were maintained on a 12-hour light-dark cycle with *ad libitum* access to standard chow (Specialty Feeds, Western Australia) and water under standard laboratory conditions (21°C).

Viruses and Surgical procedures

Mice were anesthetised using isoflurane (5% for induction, 2% for maintenance) and positioned on a stereotaxic frame (Stoelting, IL, USA). A Neuros syringe (Hamilton, Reno, NV, USA) was used to deliver virus to the target regions; bilateral LH (-1.3mm Bregma; +/- 1.0mm lateral; -4.9mm ventral from surface of brain) and mPFC (+1.55mm and +1.75mm Bregma; +/- 0.3mm lateral; -1.75mm ventral from surface of brain). Following surgery mice were given 3 weeks to recover and to ensure viral expression before experiments commenced. For viral details and specific experimental details see supplemental methods and materials.

Behavioural Testing

All behaviour experiments were video recorded and behavioural tracking analysis was performed blinded to treatment using Ethovision version 14.0.1322 (Noldus Information Technology; NL). The elevated zero maze, light dark box and open field were used to assess anxiety-like behaviour as well as novel environment and novel food stress, as described in the supplemental methods. More detailed behaviour, such as sniffing, approaching and eating food (as measured in the novel and familiar palatable food intake experiments) was scored manually by a researcher blinded to treatment group.

Feeding experimental devices 3 (FED3; Open Ephys, Portugal) were used for operant conditioning and were placed in the home cage with a divider attached to prevent mice from climbing the device [20]. FED3 reduces stress and negates the need to calorie restrict mice to learn the association between the correct nose poke and pellet delivery, an important consideration when studying the interaction between homeostatic and motivational pathways. FED3s were filled with sucrose pellets as rewards (Test Diet Sucrose tablet 20 mg, Richmond, IN, USA). For details of operant FED3 experiments see supplemental methods.

Fibre photometry recording

Mice were acclimated to the photometry recording room and connected to the tethered fibre optic cables cord (400µm core, 0.48 NA; MF1.25 connector; Doric Lenses) in their home cage within the photometry recording room for 1-hour a day for five days leading up to behaviour experiments to minimise stress associated with connecting the probe to the patch cord. Fibre optic cannulas were cleaned with 70% ethanol prior to connecting them to patch cords to minimise contamination of the signal. Two excitation wavelengths, 465nm (Ca2+-dependent signal) and 405nm (Ca2+- independent isosbestic control signal for movement artefacts) emitted from LEDs (Doric Lenses, Canada) were delivered to a dual-fluorescence minicube (4 port fluorescence minicube, FC connectors; Doric Lenses, Canada) before connecting to a rotary joint (pig-tailed 1x1 Fibre-optic rotary joint, 400µm core, 0.48 NA, FC connector; Doric Lenses, Canada) which allow for uninterrupted movement of the patch cord attached to the fibre optic cannula. GCaMP7 and isosbestic fluorescence wavelengths were collected using the same fibre optic cable and filtered back through the dichroic ports of the dual-fluorescence minicube into a femtowatt photoreceiver (model no. 2151; Newport). Synapse software (Tucker-Davis Technologies, FL, USA) controlled and modulated the excitation (465 nm: 210 Hz, 405 nm: 530 Hz), as well as demodulated and low-pass filtered (4 Hz) in real-time via the fibre photometry processer (RZ5P;Tucker-Davis Technologies). LED power was adjusted for each mouse to achieve approximately 200mV and 100mV output for GCaMP and isosbestic control signals respectively. Synapse software also integrated high-definition video recordings of mouse behaviour during experiments to allow behavioural events to be accurately time-stamped and integrated with the fluorescent signals. Following recording, behavioural events were timestamped using Open Scope software (Tucker-Davis Technologies) with the researcher blinded to the acquired fluorescent signals. Custom python code was used to integrate and analyse the fluorescent signals during behavioural events or researcher delivered stimuli.

Fibre photometry analysis

Data analysis for each experiment was performed using a customised python code (https://github.com/Andrews-Lab/Clarke-et-al-mPFC-LH-manuscript). Ca^{2}+ and isosbestic signals during recording sessions were extracted and down sampled (10 samples/s). The

isosbestic signal was fitted to the Ca^{2}+-dependent signal using a least squares polynomial fit and delta F/F was calculated using the equation: (Ca^{2+}-dependent signal - fitted isosbestic signal)/fitted isosbestic signal to correct for photobleaching of the signal and movement artefacts. Due to the short time frame of each experiment (15-45 minutes) photobleaching of the GCamp7s signal was negligible. Z-score normalisation was then calculated from the delta F/F for each trial or behavioural event using the equation: $z = (F-F\mu)/F\sigma$ where F is the signal and $F\mu$ and $F\sigma$ are the mean and standard deviation of the baseline signal. Baseline was determined to be -15 to -5 second prior to each behavioural event/stimulus presentation. Average z-scores for each trial were determined and statistically analysed in Graph Pad Prism, V 9.1.2. For details of fibre photometry experiments see supplemental methods.

Statistical Analysis

Data are expressed mean with standard error of the mean. Comparisons were tested using two-tailed unpaired t-tests or paired t-tests. A one-way ANOVA with Tukey's multiple comparison test was applied when multiple groups were compared at the same time point. A repeated measures one-way ANOVA was applied when multiple time points were compared to baseline values. A two-way ANOVA with Sidak's multiple comparison test was applied when there both fasting and fed conditions, or when a variable was measured over time. All statisitical tests used are described in figure legends with details provided in supp table 1, $p<0.05$ was considered statistically significant. Graphs were generated Graph Pad Prism, V 9.1.2.

Results

Human spDCM

At the subject-level, we used the time-series from the ROIs to define and estimate a fully connected DCM for each participant and condition using Variational Laplace [21]. The average variance explained across subject-level DCM inversion was very high (hunger: M = 93.73, SD = 1.10, range = 89.67-96.48; Satiety: M = 94.12, SD = 1.08, range = 88.19-95.97), indicating very good model fitting.

Homeostatic State (Hunger vs. Satiety).

First, we explored how homeostatic state changes the dynamic connectivity between the ACC, vmPFC and bilateral LH independent of BMI. Hunger, compared to satiety, was associated with a decreased inhibition from the vmPFC to the left (-0.101 Hz, 95% CI [-0.01,-0.20]) and right LH (-0.11 Hz, 95% CI [-0.02, -0.20]) (Figure 1A).

Body Mass Index

Next, we investigated how BMI affects the effective connectivity between ACC, vmPFC and bilateral LH whilst controlling for homeostatic state. Increased BMI was associated with a decreased excitation from the left LH to the ACC (-0.02 Hz, 95% CI [-0.002, -0.04]) (Figure 1B). Further, there was a decreased self-inhibition of the ACC associated with elevated BMI (-0.024 Hz, 95% CI [-0.01, -0.04]). This disinhibition reflects an enhanced sensitivity to inputs from connecting nodes [22], i.e. the LH, in individuals with higher BMI. There were no reliable interaction effects between BMI and homeostatic state, but weak evidence (i.e. posterior probability < 0.75) for a decreased excitation from the vmPFC to the ACC (-0.01 Hz, 95% CI [0.01, -0.03]).

Functional dissection of the mPFC-LH pathway in mice.

To functionally test the hypothesis, generated from spDCM studies in humans, that the mPFC-LH projection normally restrains feeding, we confirmed in mice that some neuronal projections to the LH in mice originate from regions analogous to the mPFC in humans. AAVrg-CAG-GFP in the LH (Fig 2B), a retrogradely transported viral vector expressing GFP, identified cells bodies in the mouse prelimbic, infralimbic and rostral cingulate gyrus 1 (Cg1) regions (Fig 2C), which we refer to as mPFC, as described previously [23, 24]. We also observed scattered cells in the insular cortex (Fig 2C), consistent with a known LH input from the insular cortex [15]. For continuity with our human data described above, we refer to projections from these regions to the LH as mPFC–LH.

Activation of the mPFC-LH pathway is anorectic and reduces motivation.

To activate this circuit, we used a dual viral approach to express the DREADD receptor hM3Dq into mPFC-LH projecting neurons (Fig 2D), following bilateral injection of a retrograde AAV expressing cre recombinase. This resulted in substantial expression of hM3Dq and mCherry in the mPFC with significantly greater Fos/mCherry co-expression after CNO (Fig 2E-F). Firstly, acute activation of the mPFC-LH circuit during the early light phase, the period when mice are typically inactive (Fig 2G), significantly suppressed food intake after 4 hours (Fig 2J). We also examined food intake following a short-term 3hr fast to normalize feeding status during the dark phase, the period when mice consume the majority of their energy intake (Fig 2H), and again acute activation of the mPFC-LH circuit significantly suppressed food intake after 4 hours (Fig 2K). Finally, we investigated whether acute mPFC-LH circuit activation could suppress feeding when mice are challenged with a longer term overnight fast (Fig 2I). Acute

circuit activation suppressed food intake at 4 hours (Fig 2L) from food being available. Together, this supports the hypothesis that the mPFC-LH projection is an anorexigenic circuit.

To assess whether the mPFC-LH pathway suppresses motivated behaviour to obtain a food reward (20mg sucrose pellet), we used a FED3 home cage operant conditioning system (Fig 2M) [20]. Mice were trained on FR1-FR3-FR5 schedules until all mice correctly selected the active nose poke 75% of total pokes performed (Fig 2N). To test for appetitive motivated behaviour, mice were subjected to a progressive ratio task following CNO injection (Fig 2O) either in a mildly fasted or ad libitum fed state at the start of the dark phase. DREADD activation of the mPFC-LH circuit suppressed operant responding, as assessed by the breakpoint reached, however the suppression of operant responding only occured in the acute 3 hr fasted state (Fig 2P-O), when mice ordinarily express increase motivation to obtain a caloric reward. As expected, fasted control animals reached higher breakpoints than control animals in the fed state, however, this was not observed after DREADD activation of the mPFC-LH circuit (Fig 2R). Moreover, acute activation of the mPFC-LH pathway did not affect anxiety-like behaviour or exploratory locomotor behaviour assessed using the elevated zero maze, open field or light-dark box (Suppl Fig 1C-H). Together with the free feeding experiments described above, our results suggest that activation of the mPFC-LH circuit directly suppresses both appetitive and consummatory feeding behaviours without affecting anxiety-like behaviour.

To further explore the role of the mPFC-LH circuit, we employed a novel wireless optogenetics approach [25] to investigate short-term manipulations of the vesicular glutamate transporter-1 (Vglut1-cre, a glutamatergic marker primarily restricted to the cortex [26]) expressing neurons following mPFC-LH circuit activation (Suppl Fig 2A; mPFC^{Vglut1}-LH). We confirmed expression of retrograde hChR2(H134R) and the mCherry reporter protein throughout the mPFC (Suppl Fig 2B). Photostimulation of the mPFC^{Vglut1}-LH pathway suppressed feeding after a 14-hour fast when stimulation was paired with returning food to the home cage (Suppl Fig 2C-D). Next, we photostimulated the mPFC^{Vglut1}-LH circuit during a real-time place preference task, in order to assess the inherent rewarding or aversive nature of this circuit (Suppl Fig 2E-H). Mice spent less time in the side of the arena paired with photostimulation in mPFC^{Vglut1}-LH photostimulation group, compared to a light-off control period (Suppl Fig 2G), which was not due to differences in locomotor activity (Suppl Fig 2H). This suggests that photostimulation of the mPFC^{Vglut1}-LH circuit conveys aversive-state information, likely contributing to the reduction in food intake. Based on these results, we hypothesised that photostimulation of the mPFC^{Vglut1}-LH circuit would suppress motivation to obtain a sucrose pellet, similar to DREADD activation studies. We trained mice in a procedure similar to that described in Fig 2N before testing acutely 3 hour fasted mice with a progressive ratio task under conditions of photostimulation and no stimulation (Suppl Fig 2I). Photostimulation of the mPFC-LH^{Vglut1} circuit suppressed breakpoint ratio reached and active nose pokes (Suppl Fig 2J) consistent with results from the DREADDs studies. Together our results support an inhibitory role for the mPFC^{Vglut1}-LH circuit on feeding and motivated reward-seeking behaviour by increasing aversive processing.

Acute stressors and food consumption modulate the mPFC-LH circuit.

In order to identify how the mPFC-LH pathway is physiologically modulated, we used *in vivo* fiber photometry coupled with our dual viral approach (Fig 3A-D). The anorexigenic nature of this circuit suggests that it may be activated by factors that attenuate feeding such as acute stressors, or inhibited under certain conditions to encourage consumption. To test this, mice were exposed to acute hand in cage stress and air puff stress. Both acute hand in cage and air puff stress increased mPFC-LH neural activity, as measured by GCaMP7s fluorescence,

resulting in an approximately 2-fold increase in the first 10 seconds after stress exposure relative to the baseline period (-15 to -5 seconds prior to stress exposure) (Fig 3E-L). The increased activity occurs with the appearance of the hand and peaks at contact with the hand (Suppl Fig C-D), similar in profile to stress-sensitive corticotropin-releasing horomone neurons [27]. Novel environments are known to produce acute anxiety-like behaviour [28] and we examined the impact of an anxiety-evoking novel environment on mPFC-LH activity. Although mPFC-LH activity increased immediately prior to entry into the novel environment, it did not vary significantly from baseline following entry into the novel environment (Fig 3O). Moreover, we noticed a significantly higher peak z-score when comparing the 2nd entry to the last entry, suggesting neural responses were reduced as animals became more familiar with the environment (Suppl Fig C-D). Similarly, we observed a greater increase in mPFC-LH activity when approaching a novel, but not familiar, object (Suppl Fig 3G-J). Collectively these results suggest that increased activity prior to entry into a novel environment or on approaching a novel object predicts a potential threat, however in the absence of a threat activity returns to baseline.

We then exposed mice to chow, familiar palatable or novel palatable foods and examined the effects on mPFC-LH activity. When mPFC-LH activity was time-stamped to food consumption, we observed a significant reduction in response to chow, familiar palatable and novel palatable foods (Fig 3U-W). We also observed a transient suppression of mPFC-LH activity in response to chewing a wooden dowel (Fig 3X), although this response was not sustained for the full 15 second period after initiating consumption, as seen with chow and palatable food (Fig 3U-W). Moreover, the change in activity occurred upon chewing/consumption and not in response to presentation of the food or wooden dowel or upon approach (S3P-S). This change was not proportional to calories consumed, palatability of food or metabolic state (Suppl Fig 3K-AB), suggesting this circuit is not part of broader neural network responding to calorie content or metabolic need.

Inhibition of the mPFC-LH pathway increases food intake.

To test if artificial inhibiton of the mPFC-LH pathway could also suppress food consumption, we expressed the inhibitory DREADD receptor hM4Di into mPFC-LH projecting neurons (Figure 4A). Cre-dependent mCherry and hM4Di expression was observed in the mPFC, and fos activity was significantly reduced in hM4Di expressing animals compared to controls following CNO (Fig 4B-C). Inhibtion of the mPFC-LH pathway did not affect home cage food intake in the light phase (Fig 4D, G), after an acute 3 hour fast at the beginning of the dark phase (Fig 4E, H) or after a 14-hour fast (Fig 4F, I). Similarly, motivated home cage food-seeking as assessed with a progressive ratio with FED3 showed no differences in breakpoint reached during either fed and fasted conditions (Fig 4J-K). To examine the role of stress/novelty in the effects of mPFC-LH inhibition on motivated behaviour, we conducted a PR in a novel environment (Fig 4L) and observed that breakpoint responding was suppressed during the first 5 minutes compared to the home cage (Fig 4M), confirming that actue stress transiently affects motivated reward seeking. Intriguingly, inhibition of the mPFC-LH pathway with hM4Di significantly increased breakpoint reached within the first 5 minutes of the PR in a novel environment (Fig 4M). Moreover, mPFC-LH inhibition promoted the consumption of familiar palatable food in a novel environment, reduced latency to first eating bout and increased time spent eating in a novel environment (Fig 4N-R). We also observed similar effects when novel palatable food was given in a familiar environment, including increased food consumption, number of eating bouts, time spent eating and less time outside of the food zone (Fig 4S-W). No differences in anxiety-like behaviour was observed in the elevated zero maze or light dark box, and no differences in locomotor activity was observed in the open field (Suppl Fig 4). Collectively, these results suggest that mPFC-LH inhibiton alleviates stress-

induced avoidance of novel food or food in a novel environment and promotes reward seeking and food consumption.

Ablation of the mPFC-LH pathway increases body weight gain

The results presented above highlight that the mPFC-LH circuit is an anorectic pathway that is sensitive to acute stress. In order to test the prediction, based on the findings above, that chronic ablation of an anorexigenic mPFC-LH pathway would affect long-term body weight, cre-dependent caspase was injected into the mPFC following injection of retrograde CAV2-cre into the LH (Fig 5A). Chronic ablation of the mPFC-LH circuit was confirmed by reduced NeuN immunoreactivity in the mPFC (Fig 5B). mPFC-LH caspase ablated mice were significantly heavier compared to baseline 3 weeks after injection and when followed for 14 weeks post injection (Fig 5C), despite a number of procedural events during this time that resulted in specific periods of acute body weight loss in both experimental groups. Although standard chow diet consumption was not different over 24 hours, mPFC-LH caspase ablated mice consumed more novel high fat/high sugar diet over 24 hours (Fig 5H). Moreover, chronc ablation of the mPFC-LH circuit did not affect anxiety-like behaviour or locomotor activity when measured in the elevated plus maze or open field (Suppl Fig 5). Thus, these results highlight that chronic ablation of the mPFC-LH promotes consumption of a novel HFD and causes weight gain on a chow diet.

Discussion

The neuronal control of food intake is essential for the maintenance of a healthy body weight and involves a complex interplay between homeostatic, motivational and cognitive drivers. Here, we identified a previously uncharacterised neuronal pathway related to hunger and satiety in humans and interrogated the function of this pathway with respect to feeding and motivated behaviour in mouse models. We show that the powerful inhibitiory influence from the mPFC to LH is absent in humans while hungry and that this same mPFC-LH circuit is both stress-sensitive and anorexigenic in mice. This reverse translational approach to understanding the neural control of food seeking and consumption overcomes specific shortcomings that often hamper translational research in metabolic neuroscience and offers a powerful template for future studies.

In the present study, the strength of connectivity between mPFC-LH was reduced in states of hunger regardless of BMI. This observation is noteworthy considering human neuroimaging studies implicate hyperactivation of the mPFC in obesity [10, 29] as well as anorexia nervosa [11, 30], which are at opposite ends of the BMI spectrum. The mPFC is a brain region implicated in a broad range of responses that includes the encoding of cue- and value-association, and decision making related to reward-seeking [10, 29]. Intriguingly, activation of mPFC neurons can either promote or suppress reward responding depending on the projection specific population targeted, as well as the behavioural paradigm examined [23, 31]. With this in mind, it is not surprising that human neuroimaging studies report that the mPFC is hyperactive in both extremes of body weight disturbance suggesting it is likely to be involved in neural processes that override homeostatic signals. The diverse function of the mPFC in feeding and reward processing is at least partly explained by its broad neuronal projection profile, including well-studied projections to the nucleus accumbens (NAc) , ventral tegmental area (VTA), paraventricular thalamus (PVT) and basolateral amygdala (BLA) [23, 31 , 32]. Although anatomical mPFC projections to the LH have been previously described [33, 34], the function of this circuit remains to be described, with the only functional study suggesting a role in aggressive behaviour in response to changing social threats [35]. Consistent with previous anatomical reports, we show mPFC neurons project from the PrL, IL and Cg1 subregions of the mPFC directly to the LH. Our results demonstrate that the functional role of the mPFC to LH circuit is anorexigenic, suppressing food intake and motivation to consume palatable food. Specifically, either acute chemogentic activation of the mPFC-LH circuit or optogentic activation of $mPFC^{Vglut1}$-LH neurons suppressed both food intake and motivation to obtain palatable food. These findings are in line with evidence that other cortical inputs into the LH, for example, the anterior insula cortex, alters feeding behaviour and body weight maintenance [15].

The mPFC-LH pathway was also engaged by acute stressors in this study, a finding that is supported by a known role of the mPFC in integration of acute stress [36, 37, 38]. This study moves beyond the observation that acute stress increases mPFC activity and illustrates that acute stress recruits the mPFC-LH pathway to suppress food intake and motivation for sucrose pellets. Moreover, the activity of this pathway appears to *predict* acute stress, as shown by the recruitment of mPFC-LH neuons immediately prior to entry into a novel environment or on approach of a novel object. The predictive nature of this pathway is only apparent when mice make the decision to enter or approach, consistent with the notion that mPFC neurons are important in decision-making [39, 40, 41] and event or threat prediction [42, 43, 44, 45, 46]. Furthermore, this prediction-like activity diminished over subsequent events, suggesting that prior experience updates the predictive function of this circuit. Similar habituation in response to stress experience has been observed in CRH neurons [47]. This circuit is specifically relevant to acute stress, rather than a persistent trait of generalized anxiety, because circuit manipulation had no affect anxiety-like behaviour.

Food consumption, but not food presentation or approach reduced mPFC-LH activity and, surpisingly, the magnitude of the fall was not related to metabolic state, palatability or food consumed, as has been observed with hunger-sensing AgRP neurons [48]. Moreover, chewing a wooden dowel elicited a similar fall in activity, although not to the same extent as palatable food. Altered PFC activity has been observed in response to palatable food consumption in models of binge eating [49], suggesting that this circuit may play an important role regulating emotional state in the absence of homeostatic need. In support of this, mPFC-LH DREADD inhibiton increased acute motivated reward-seeking, food approach and consumption, only under conditions of mild stress, such as in a novel environment or in response to a novel food [50] and not home cage feeding.

There is conflicting data on the role of the mPFC in cue-dependent learning, value association and motivation to seek reward. For example, mPFC activity is associated with the inhibition of motivated, natural and drug-related reward seeking [23, 51, 52, 53, 54]. However, opposing results suggest that mPFC activity drives responding for natural and drug-related rewards and also reinstatement of cue-induced or context-induced reward seeking following extinction [31, 32, 55, 56]. It is worth reiterating that human neuroimaging studies also report discrepancies in mPFC activity with hyperactivation in both obesity [10, 29] and anorexia nervosa [11, 30]. These differences may be largely explained by the projection targets of the mPFC neurons in question, in which corticostriatal pathways increase reward seeking and corticothalamic pathways inhibit reward seeking [31]. Our results build upon this model by including corticohypothalamic pathways as an inhibitory pathway specific for food-related reward seeking. Supporting this idea and relevant to the feeding experiments herein, photostimulation of mPFC dopamine 1 receptor-expressing neurons, which project to both striatal and limbic regions, promotes food intake and responding for food reward [32]. While the corticostriatal circuit was not explicitly examined in this study, the activation of the corticolimbic neurons is sufficient to increase food intake [32]. Other studies have demonstrated that activation of corticolimbic circuits promotes reward seeking [57]. Possibly, mPFC limbic and striatal projections have similar roles in promoting reward seeking, while thalamic and hypothalamic projections generally act to suppress food intake and motivated behaviours. Although it is important to note that within each projection specific population of mPFC neurons (striatal or thalamic) there is diversity in activity profiles in response to cues that predict reward [31]. While it may be possible to generalize about the role of mPFC projections, there are likely smaller subsets of neurons with in each projection specific population that have opposing functions.

An interaction between the PFC and LH, involving orexin neurons, is required for cue-potentiated feeding to increase food motivation and food cue memory. [58, 59, 60]. Moreover, pharmacological inhibition of the mPFC with intra-mPFC injection of DAMGO, a μ-opioid receptor agonist, induces feeding, increases progressive ratio responding for sucrose rewards and increases locomotor activity [61], similar to our observation using acute Gi DREADD inhibition mPFC-LH pathway. Intra-mPFC injection of DAMGO also increased fos expression in orexin neurons [61], suggesting the presence of an indirect circuit from the mPFC to LH, as DAMGO inhibition would not induce fos expression, a marker of increased activity [62], in LH orexin neurons. A possible indirect route from the mPFC-LH involves somatostatin neurons in the lateral septum [63].

These studies rasie an important question; what are the downstream targets of LH neurons from mPFC? Photostimulation of LH^{Vgat} neurons, which are molecularly distinct from orexin and melanin concentrating hormone (MCH) expressing neurons, increases consumption of food in fed animals, while photoinhibition has the opposite effect [64]. In contrast, photostimulation of LH^{Vglut2} neurons suppresses food intake in fasted animals and is aversive [65]. Further supporting these studies, genetic ablation of LH^{Vglut2} neurons increases body weight

gain and calories consumed on a palatable diet [66]. Our chemogenetic, optogenetic and circuit ablation approaches directly phenocopy studies manipulating LH^{Vglut2} neurons. An important recent study shows that LH^{Vgat} and LH^{Vglut2} neurons are not sensitive to interoceptive signals of homeostatic state [67], supporting our observations that the mPFC-LH neural activity in response to food is also not sensitive to hunger. We predict that LH^{Vglut2} neurons are a primary downstream target of excitatory mPFC^{Vglut1} LH projecting neurons. Indeed, a recent set of studies show that LH^{Vglut2} neurons form part of a neural circuit that can suppress hunger-sensing AgRP neurons via a GABAergic population in the the dorsal medial hypothalamic nucleus [68]. In addition, neurons from the mPFC (PrL and IL) have monosynaptic inputs with orexin and melanin-concentrating hormone neurons in the LH and these neuronal populations are differentially affected by air puff stress, immobilisation or novel object presentation and investigation [69].

Other cortical inputs to the LH including the insular cortex also modulate feeding and behaviour [15], with effects that are strikingly similar to ours and suggest that direct cortical inputs to the LH provide anorexigenic and aversive information that is independent of homeostatic drive. Indeed, the mPFC-LH circuit may play important and underappreciated roles in the pathogenesis of psychometabolic conditions at opposite ends of the body weight sprectrum. For example, excessive cognitive control related to increased mPFC activity is associated with anorexia nervosa [11] and excessive dietary self control [6], while chronic inhibiton of the mPFC reduces anorectic symptoms in a rat model of activity-based anorexia [70]. On the other hand, decreased activity upon consumption removes this restraint and may, in some circumstances, promote body weight gain. This idea is supported in the present study, whereby mPFC-LH circuit ablation resulted in increased bodyweight on a chow diet and increased acute consumption of palatable food. While this might be an important new target to combat overeating associated with the progression to obesity, its important to note that human neural network modelling did not identify BMI as a factor affecting mPFC-LH activity.

In summary, we have used a combination of human imaging and network modelling, together with neural circuit control in mice, to identify a previously uncharacterized mPFC-LH pathway involved in the regulation of food intake and motivation. Neural recordings using photometry revealed that this pathway responds to acute stressors and predicts potential stress/threat when animals voluntarily enter a novel environment or approach a novel object. Intriguingly, this stress-sensitive pathway is suppressed in response to food consumption but not affected by metabolic state or palatability, which establishes a novel neural pathway that may provide top-down cortical control over food intake and motivation, independent of hunger or energy needs. Future studies are required to elucidate the environmental, developmental, psychological and physiological cues affecting this system as they might play important roles in the pathogenesis of opposing psychometabolic conditions such as anorexia nervosa or overeating and obesity.

References

1. Locke AE*, et al.* Genetic studies of body mass index yield new insights for obesity biology. *Nature* **518**, 197-U401 (2015).

2. O'Rahilly S, Farooqi IS. Human obesity as a heritable disorder of the central control of energy balance. *Int J Obes (Lond)* **32 Suppl 7**, S55-61 (2008).

3. Andermann ML, Lowell BB. Toward a Wiring Diagram Understanding of Appetite Control. *Neuron* **95**, 757-778 (2017).

4. Kanoski SE. Cognitive and neuronal systems underlying obesity. *Physiology & Behavior* **106**, 337-344 (2012).

5. Boswell RG, Kober H. Food cue reactivity and craving predict eating and weight gain: a meta-analytic review. *Obesity Reviews* **17**, 159-177 (2016).

6. Hare TA, Camerer CF, Rangel A. Self-Control in Decision-Making Involves Modulation of the vmPFC Valuation System. *Science* **324**, 646-648 (2009).

7. Harding IH*, et al.* Brain substrates of unhealthy versus healthy food choices: influence of homeostatic status and body mass index. *Int J Obes (Lond)* **42**, 448-454 (2018).

8. Brooks SJ, Cedernaes J, Schioth HB. Increased Prefrontal and Parahippocampal Activation with Reduced Dorsolateral Prefrontal and Insular Cortex Activation to Food Images in Obesity: A Meta-Analysis of fMRI Studies. *PLoS One* **8**, (2013).

9. Kennedy J, Dimitropoulos A. Influence of feeding state on neurofunctional differences between individuals who are obese and normal weight: A meta-analysis of neuroimaging studies. *Appetite* **75**, 103-109 (2014).

10. Stoeckel LE, Weller RE, Cook EW, 3rd, Twieg DB, Knowlton RC, Cox JE. Widespread reward-system activation in obese women in response to pictures of high-calorie foods. *NeuroImage* **41**, 636-647 (2008).

11. Uher R*, et al.* Medial prefrontal cortex activity associated with symptom provocation in eating disorders. *Am J Psychiat* **161**, 1238-1246 (2004).

12. Misic B, Sporns O. From regions to connections and networks: new bridges between brain and behavior. *Current opinion in neurobiology* **40**, 1-7 (2016).

13. Alhadeff AL, Goldstein N, Park O, Klima ML, Vargas A, Betley JN. Natural and Drug Rewards Engage Distinct Pathways that Converge on Coordinated Hypothalamic and Reward Circuits. *Neuron* **103**, 891-+ (2019).

14. Mazzone CM*, et al.* High-fat food biases hypothalamic and mesolimbic expression of consummatory drives. *Nature Neuroscience* **23**, 1253-+ (2020).

15. Wu Y*, et al.* The anterior insular cortex unilaterally controls feeding in response to aversive visceral stimuli in mice. *Nature communications* **11**, (2020).

16. Nieh EH*, et al.* Inhibitory Input from the Lateral Hypothalamus to the Ventral Tegmental Area Disinhibits Dopamine Neurons and Promotes Behavioral Activation. *Neuron* **90**, 1286-1298 (2016).

17. Kullmann S*, et al.* Resting-State Functional Connectivity of the Human Hypothalamus. *Human brain mapping* **35**, 6088-6096 (2014).

18. Contreras-Rodriguez O, Vilar-Lopez R, Andrews ZB, Navas JF, Soriano-Mas C, Verdejo-Garcia A. Altered cross-talk between the hypothalamus and non-homeostatic regions linked to obesity and difficulty to lose weight. *Scientific reports* **7**, 9951 (2017).

19. Buckner RL, Krienen FM, Yeo BTT. Opportunities and limitations of intrinsic functional connectivity MRI. *Nature Neuroscience* **16**, 832-837 (2013).

20. Matikainen-Ankney BA*, et al.* Feeding Experimentation Device version 3 (FED3): An open-source home-cage compatible device for measuring food intake and operant behavior. *eLife* **10.7554/eLife.66173**, (2021).

21. Friston KJ, Mattout J, Trujillo-Barreto N, Ashburner J, Penny W. Variational free energy and the Laplace approximation. *NeuroImage* **34**, 220-234 (2007).

22. Friston KJ, Harrison L, Penny W. Dynamic causal modelling. *NeuroImage* **19**, 1273-1302 (2003).

23. Kim CK*, et al.* Molecular and Circuit-Dynamical Identification of Top-Down Neural Mechanisms for Restraint of Reward Seeking. *Cell* **170**, 1013-+ (2017).

24. Laubach M, Amarante LM, Swanson K, White SR. What, If Anything, Is Rodent Prefrontal Cortex? *Eneuro* **5**, (2018).

25. Shin G*, et al.* Flexible Near-Field Wireless Optoelectronics as Subdermal Implants for Broad Applications in Optogenetics. *Neuron* **93**, 509-+ (2017).

26. Zeisel A*, et al.* Molecular Architecture of the Mouse Nervous System. *Cell* **174**, 999-+ (2018).

27. Daviu N*, et al.* Paraventricular nucleus CRH neurons encode stress controllability and regulate defensive behavior selection. *Nat Neurosci* **23**, 398-410 (2020).

28. Merali Z, Levac C, Anisman H. Validation of a simple, ethologically relevant paradigm for assessing anxiety in mice. *Biol Psychiatry* **54**, 552-565 (2003).

29. Schur EA, Kleinhans NM, Goldberg J, Buchwald D, Schwartz MW, Maravilla K. Activation in brain energy regulation and reward centers by food cues varies with choice of visual stimulus. *Int J Obes (Lond)* **33**, 653-661 (2009).

30. Ellinson Z, Foong J, Howard R, Bullmore E, Williams S, Treasure J. Functional anatomy of calorie fear in anorexia nervosa. *Lancet* **352**, 1192-1192 (1998).

31. Otis JM*, et al.* Prefrontal cortex output circuits guide reward seeking through divergent cue encoding. *Nature* **543**, 103-+ (2017).

32. Land BB*, et al.* Medial prefrontal D1 dopamine neurons control food intake. *Nat Neurosci* **17**, 248-253 (2014).

33. Barone FC, Wayner MJ, Scharoun SL, Guevaraaguilar R, Aguilarbaturoni HU. Afferent Connections to the Lateral Hypothalamus - a Horseradish-Peroxidase Study in the Rat. *Brain research bulletin* **7**, 75-88 (1981).

34. Hahn JD, Swanson LW. Distinct patterns of neuronal inputs and outputs of the juxtaparaventricular and suprafornical regions of the lateral hypothalamic area in the male rat. *Brain Res Rev* **64**, 14-103 (2010).

35. Biro L*, et al.* Task Division within the Prefrontal Cortex: Distinct Neuron Populations Selectively Control Different Aspects of Aggressive Behavior via the Hypothalamus. *Journal of Neuroscience* **38**, 4065-4075 (2018).

36. McKlveen JM, Myers B, Herman JP. The Medial Prefrontal Cortex: Coordinator of Autonomic, Neuroendocrine and Behavioural Responses to Stress. *J Neuroendocrinol* **27**, 446-456 (2015).

37. Uribe-Marino A*, et al.* Prefrontal Cortex Corticotropin-Releasing Factor Receptor 1 Conveys Acute Stress-Induced Executive Dysfunction. *Biological Psychiatry* **80**, 743-753 (2016).

38. Radley JJ, Arias CM, Sawchenko PE. Regional differentiation of the medial prefrontal cortex in regulating adaptive responses to acute emotional stress. *Journal of Neuroscience* **26**, 12967-12976 (2006).

39. Luk CH, Wallis JD. Dynamic encoding of responses and outcomes by neurons in medial prefrontal cortex. *J Neurosci* **29**, 7526-7539 (2009).

40. Schmidt B, Duin AA, Redish AD. Disrupting the medial prefrontal cortex alters hippocampal sequences during deliberative decision making. *J Neurophysiol* **121**, 1981-2000 (2019).

41. Kaplan R, Schuck NW, Doeller CF. The Role of Mental Maps in Decision-Making. *Trends Neurosci* **40**, 256-259 (2017).

42. Alexander WH, Brown JW. A general role for medial prefrontal cortex in event prediction. *Front Comput Neurosci* **8**, 69 (2014).

43. Fisher PM*, et al.* Medial prefrontal cortex serotonin 1A and 2A receptor binding interacts to predict threat-related amygdala reactivity. *Biol Mood Anxiety Disord* **1**, 2 (2011).

44. Liu L, Zhang L, Wang T, Chen L. Dopamine D1 receptor in the medial prefrontal cortex mediates anxiety-like behaviors induced by blocking glutamatergic activity of the ventral hippocampus in rats. *Brain Res* **1704**, 59-67 (2019).

45. Parfitt GM*, et al.* Bidirectional Control of Anxiety-Related Behaviors in Mice: Role of Inputs Arising from the Ventral Hippocampus to the Lateral Septum and Medial Prefrontal Cortex. *Neuropsychopharmacology* **42**, 1715-1728 (2017).

46. Pratt WE, Mizumori SJ. Neurons in rat medial prefrontal cortex show anticipatory rate changes to predictable differential rewards in a spatial memory task. *Behav Brain Res* **123**, 165-183 (2001).

47. Kim JS, Han SY, Iremonger KJ. Stress experience and hormone feedback tune distinct components of hypothalamic CRH neuron activity. *Nature communications* **10**, 5696 (2019).

48. Chen Y, Lin YC, Kuo TW, Knight ZA. Sensory detection of food rapidly modulates arcuate feeding circuits. *Cell* **160**, 829-841 (2015).

49. Sinclair EB, Klump KL, Sisk CL. Reduced Medial Prefrontal Control of Palatable Food Consumption Is Associated With Binge Eating Proneness in Female Rats. *Frontiers in behavioral neuroscience* **13**, 252 (2019).

50. Blasco-Serra A, Gonzalez-Soler EM, Cervera-Ferri A, Teruel-Marti V, Valverde-Navarro AA. A standardization of the Novelty-Suppressed Feeding Test protocol in rats. *Neurosci Lett* **658**, 73-78 (2017).

51. Chen BT*, et al.* Rescuing cocaine-induced prefrontal cortex hypoactivity prevents compulsive cocaine seeking. *Nature* **496**, 359-+ (2013).

52. Ferenczi EA*, et al.* Prefrontal cortical regulation of brainwide circuit dynamics and reward-related behavior. *Science* **351**, (2016).

53. Jonkman S, Mar AC, Dickinson A, Robbins TW, Everitt BJ. The Rat Prelimbic Cortex Mediates Inhibitory Response Control But Not the Consolidation of Instrumental Learning. *Behavioral neuroscience* **123**, 875-885 (2009).

54. Pfarr S*, et al.* Losing Control: Excessive Alcohol Seeking after Selective Inactivation of Cue-Responsive Neurons in the Infralimbic Cortex. *Alcohol Alcoholism* **50**, (2015).

55. Bossert JM*, et al.* Role of Projections from Ventral Medial Prefrontal Cortex to Nucleus Accumbens Shell in Context-Induced Reinstatement of Heroin Seeking. *Journal of Neuroscience* **32**, 4982-4991 (2012).

56. McFarland K, Davidge SB, Lapish CC, Kalivas PW. Limbic and motor circuitry underlying footshock-induced reinstatement of cocaine-seeking behavior. *Journal of Neuroscience* **24**, 1551-1560 (2004).

57. Malvaez M, Shieh C, Murphy MD, Greenfield VY, Wassum KM. Distinct cortical-amygdala projections drive reward value encoding and retrieval. *Nat Neurosci* **22**, 762-769 (2019).

58. Cole S, Keefer SE, Anderson LC, Petrovich GD. Medial Prefrontal Cortex Neural Plasticity, Orexin Receptor 1 Signaling, and Connectivity with the Lateral Hypothalamus Are Necessary in Cue-Potentiated Feeding. *Journal of Neuroscience* **40**, 1744-1755 (2020).

59. Cole S, Mayer HS, Petrovich GD. Orexin/Hypocretin-1 Receptor Antagonism Selectively Reduces Cue-Induced Feeding in Sated Rats and Recruits Medial Prefrontal Cortex and Thalamus. *Scientific reports* **5**, (2015).

60. Cole S, Hobin MP, Petrovich GD. Appetitive Associative Learning Recruits a Distinct Network with Cortical, Striatal, and Hypothalamic Regions. *Neuroscience* **286**, 187-202 (2015).

61. Mena JD, Selleck RA, Baldo BA. Mu-Opioid Stimulation in Rat Prefrontal Cortex Engages Hypothalamic Orexin/Hypocretin-Containing Neurons, and Reveals Dissociable Roles of Nucleus Accumbens and Hypothalamus in Cortically Driven Feeding. *Journal of Neuroscience* **33**, 18540-18552 (2013).

62. Hoffman GE, Smith MS, Verbalis JG. C-Fos and Related Immediate-Early Gene-Products as Markers of Activity in Neuroendocrine Systems. *Front Neuroendocrinol* **14**, 173-213 (1993).

63. Carus-Cadavieco M*, et al.* Gamma oscillations organize top-down signalling to hypothalamus and enable food seeking. *Nature* **542**, 232-236 (2017).

64. Jennings JH*, et al.* Visualizing hypothalamic network dynamics for appetitive and consummatory behaviors. *Cell* **160**, 516-527 (2015).

65. Jennings JH*, et al.* Distinct extended amygdala circuits for divergent motivational states. *Nature* **496**, 224-228 (2013).

66. Stamatakis AM, Van Swieten M, Basiri ML, Blair GA, Kantak P, Stuber GD. Lateral Hypothalamic Area Glutamatergic Neurons and Their Projections to the Lateral Habenula Regulate Feeding and Reward. *Journal of Neuroscience* **36**, 302-311 (2016).

67. Siemian JN, Arenivar MA, Sarsfield S, Aponte Y. Hypothalamic control of interoceptive hunger. *Current Biology* **31**, 1-13 (2021).

68. Berrios J*, et al.* Food cue regulation of AGRP hunger neurons guides learning. *Nature* **595**, 695-700 (2021).

69. Gonzalez JA, Iordanidou P, Strom M, Adamantidis A, Burdakov D. Awake dynamics and brain-wide direct inputs of hypothalamic MCH and orexin networks. *Nature communications* **7**, 11395 (2016).

70. Milton LK*, et al.* Suppression of Corticostriatal Circuit Activity Improves Cognitive Flexibility and Prevents Body Weight Loss in Activity-Based Anorexia in Rats. *Biological Psychiatry*, (2020).

Figure Legends

Figure 1 - Second level spDCM results. (A) Effective connectivity of hunger as compared to satiety. Hunger was associated with decreased inhibition from the ventromedial prefrontal cortex to the bilateral lateral hypothalamus. (B) Effective connectivity of BMI. BMI was associated with decreased excitation from the left lateral hypothalamus to the anterior cingulate cortex (ACC) and decreased inhibition within the ACC. + or – signs code the activity state of connectivity: –, inhibitory; +, excitatory. Coloured arrows indicate connectivity strength with a decrease shown in red and an increase in green.

Figure 2. Chemogenetic activation of the mPFC-LH circuit in mice suppresses food intake and reward seeking. **A** Schematic illustrating LH target sites for retrograde tracing (left) and the regions of the mouse mPFC where projecting neurons are observed (right): Cg1, Cingulate gyrus 1; PrL, Prelimbic cortex; and IL, Infralimbic cortex. **B** Representative coronal section of LH following injection of AAVrg-CAG-GFP (green) with DAPI staining (blue). DMH, Dorsal medial hypothalamus; VMH, Ventral medial hypothalamus; ARC, Arcuate nucleus of the hypothalamus. **C** Representative coronal section showing expression of GFP (green), with DAPI staining (blue), throughout the Cg1, PrL and IL regions of the mPFC following bilateral injection of AAVrg-CAG-GFP into the LH. AID, Agranular insular cortex dorsal part; AIV, Agranular insular cortex ventral part; DP, Dorsal penduncular cortex. **D** Schematic illustrating the viral injection strategy for chemogenetic activation of mPFC-LH projecting neurons using hM3Dq-mCherry DREADDs. Control mice received an injection of a cre-dependent virus encoding for the mCherry reporter protein only. **E** Representative coronal sections of mPFC collected 90 minutes after intraperitoneal injection (i.p.) of CNO (1mg/kg). Immunofluorescent staining shows m-Cherry (red) and c-Fos (green), a marker of neuronal activity. Co-expression is indicated by white arrows.. **F** Percentage co-expression of reporter protein and Fos (n=9 for control, n=7 for mPFC-LH hM3Dq, two-tailed unpaired t-test, p=0.0033). **G-I** Schematics illustrating the experimental timelines for food intake experiments performed under varying conditions and phases of the light-dark cycle. CNO (1mg/kg) was injected 30 mins prior to the beginning of each experiment (red arrow). **J-L** Activation of mPFC-LH projecting neurons significantly reduced food intake at 4 hours in all food intake experiments (n=9-11 for control, n=7-9 for mPFC-LH hM3Dq, two-way ANOVA with Sidak's multiple comparison test; see supplementary table 2 for details). **J** There was a significant main effect of group on food intake in the light phase (control>mPFC-LH hM3Dq, p=0.035) and a significant group-by-time interaction (p=0.0082). Food intake was significantly reduced in the mPFC-LH hM3Dq group compared to control at 4 hours during the light phase experiment (p=0.0019), at 4 hours during the dark phase experiment (p=0.0461) **K**, and at 4 hours in during the fasting re-feeding experiment (p=0.0287) **L**. **M** Diagram illustrating FED3 used for the home cage operant conditioning experiments. **N** Mice were trained for 7 days prior to the progressive ratio task on fixed ratios 1-5 (n=8 for control; n=7 for mPFC-LH hM3Dq). All mice achieved an average correct response rate (% nose pokes to active side of FED3) of greater than 75% and were included in the progressive ratio task. **O** Schematic illustrating the experimental timeline for the progressive ratio task. All mice were tested in an *ad lib* fed state and following a short fast in sessions separated by one week. Mice were counterbalanced to the order of treatment. See methods for details. **P** Breakpoint ratio did not differ between groups in the fed state (two-way ANOVA, p=0.4893) however there was a significant group-by-time interaction (two-way ANOVA, p<0.0001). **Q** In the fasted state there was a main effect of group on breakpoint ratio reached (two-way ANOVA, control>mPFC-LH hM3Dq, p=0.0388) and a significant group-by-time interaction (two-way ANOVA, p<0.0001). Breakpoint ratio was significantly reduced in the

mPFC-LH hM3Dq group compared to control from 4 hours and 2 minutes to 5 hour time points (two-way ANOVA with Sidak's multiple comparison test, $p<0.05$). **R** At 5 hours from the start of the progressive ratio task, the mPFC-LH hM3Dq group reached a significantly lower breakpoint ratio compared to controls ($p=0.0004$) and there was a significant group-by-metabolic state interaction ($p=0.0001$). All data are mean ± SEM. Dots represent individual animals. For statistical analysis, a indicates a significant main effect of group, b indicates a significant interaction, *$p<0.05$ and **$p<0.01$ for between group comparisons. CNO, clozapine-N-Oxide; FED3, feeding experimentation device version 3; GFP, green fluorescent protein, LH, lateral hypothalamus; mPFC, medial pre-frontal cortex.

Figure 3. Acute stressors and food consumption modulate the mPFC-LH circuit. **A** Schematic illustrating the viral approach used to record from mPFC-LH projecting neurons. **B** Representative image showing GCaMP7s expression in mPFC-LH projecting neurons and fibre optic cannula placement. Cg1, Cingulate gyrus 1; DP, Dorsal penduncular cortex; fmi, forceps minor of the corpus callosum, IL, Infralimbic cortex; and PrL, Prelimbic cortex. **C** Fiber photometry approach used to monitor neural activity in mPFC-LH projecting neurons with 405 nm light used as an isosbestic control for motion artefact. **D** Short trace demonstrating calcium-dependent fluorescence associated with GCaMP7s (465 nm) and calcium-independent fluorescence associated with the isosbestic control (405 nm). **E** Hand in cage experiments (n=5 mice, n=3 trials per animal, 15 trials in total). **F** mPFC-LH projecting neurons are acutely activated by a hand in cage stressor. **G** Average z-score was significantly greater 0-10 seconds after hand entered cage compared to -15- -5 seconds (baseline period) prior to hand in cage (two-tailed paired t-test, $p<0.0001$). **H** Heat maps showing individual trial responses to a hand in cage test in in order of trial. **I** Response to airpuff stressor (n=4 mice, n =3 trials per animal, 12 trials in total). **J** mPFC-LH projecting neurons are acutely activated by an airpuff stressor. **K** Average z-score was significantly greater 0-10 seconds after hand entered cage compared to -15- -5 seconds (baseline period) prior to hand in cage (two-tailed paired t-test, $p=0.0009$). **L** Heat maps showing individual trial responses to airpuff in order of trial. **M** Novel environment stressor (n=6 mice, n=9 entries per animal, 54 trials in total) **N** mPFC-LH projecting neuron activity increases prior to voluntary entry to a novel environment. **O** Average z-score is significantly greater -5-0s before entering the novel arena compared to -10- -5s (baseline period) before entry (repeated measures one-way ANOVA with dunnet's multiple comparison test, -5 to 0s>-10- -5s, $p=0.0015$). **P** Heat maps showing individual trials of novel environment entry in order of trial. **Q** Neurons projecting from the mPFC-LH are suppressed by the consumption of chow (n=3 mice, n=2-8 trials per animal, 13 trials in total), **R** familiar palatable food (n=3 mice, n=5-10 trials per animal, 23 trials in total), **S** and novel palatable food (n=3 mice, n=2-4 trials per animal, 9 trials in total). **T** Chewing on a non-food object (wooden dowel) transiently suppresses mPFC-LH neural activity (n=3 mice, n = 1-4 trials per animal, 9 trials in total). **U** Average z-score was significantly reduced 0-5s, 5-10s, and 10-15s following consumption of chow compared to -10- -5s (baseline period) before consumption (repeated measures one-way ANOVA with dunnet's multiple comparison test: -10- -5s>0 -5s, $p=0.0073$; -10 -5s>5-10s, $p=0.0004$; -10- -5s>10-15s, $p=0.0004$). **V** Average z-score was significantly greater -5-0s prior to consumption of a familiar palatable food, and significantly reduced at 0-5s, 5-10s and 10-15s following consumption of a familiar palatable food compared to -10 -5s (baseline period) before consumption (repeated measures one-way ANOVA with dunnet's multiple comparison test: -5-0s>-10- -5s, $p=0.0058$; -10- -5s>0 -5s, $p=0.026$; -10 -5s>5-10s, $p<0.0001$; -10- -5s>10-15s, $p<0.0001$). **W** Average z-score was significantly reduced at 5-10s and 10-15s following consumption of a novel palatable food

compared to -10- -5s (baseline period) before consumption (repeated measures one-way ANOVA with dunnet's multiple comparison test: -10 -5s>0-5s, p=0.0166; -10 -5s>5-10s, p=0.0025; -10- -5s>10-15s, p=0.0092). **X** Average z-score was significantly reduced at 5-10s following consumption of wooden dowel compared to -10- -5s prior to consumption (repeated measures one-way ANOVA with dunnet's multiple comparison test: -10 -5s>5-10s, p=0.0275). **Y-AB** Heatmaps showing individual trials for consumption of chow, familiar palatable food, novel palatable food, and wooden dowel in order of trial. All data are mean +/- SEM. Circles represent individual trials. Dashed lines at 0 (**F**, **J**, **N**, **Q-T**) and solid lines at 0 (**H**, **L**, **P**, **Y-AB**) indicate time at which stimulus was delivered or event occurred. *p<0.05, ** p<0.01, *** p<0.001, **** p<0.0001. LH, lateral hypothalamus; mPFC, medial pre-frontal cortex.

Figure 4. Chemogenetic inhibition of the mPFC-LH circuit promotes feeding and reward seeking in stressful conditions. A Schematic illustrating the viral injection strategy for chemogenetic inhibition of mPFC-LH projecting neurons using hM4Di-mCherry DREADDs. Control mice received an injection of a cre-dependent virus encoding for the mCherry reporter protein only. **B** Representative coronal sections of mPFC from collected 90 minutes after intraperitoneal injection (i.p.) of CNO (3mg/kg). Immunofluorescent staining shows m-Cherry (red) and c-Fos (green), a marker of neuronal activity with co-expression is indicated bywhite arrows **C** Percentage co-expression of reporter protein and Fos (n=6 for control, n=7 for mPFC-LH hM4Di, two-tailed unpaired t-test, p=0.0049). **D-F** Schematics illustrating the experimental timelines for food intake experiments performed under varying conditions and phases of the light-dark cycle. CNO (3mg/kg) was injected 30 mins prior to the beginning of each experiment (red arrow). **G-I** Inhibition of mPFC-LH projecting neurons had no effect on feeding in the home cage at any stage of the light-phase or following an overnight fast (n=7-11 for control, n=5-7 for mPFC-LH hM4Di, two-way ANOVA). **J** Schematic illustrating the experimental timeline for the progressive ratio task. All mice were tested in an *ad lib* fed state and following a short fast in sessions separated by one week. Mice were counterbalanced to the order of treatment. See methods for details. **K** Inhibition of mPFC-LH projecting neurons in the home cage had no effect on breakpoint ratio in the progressive ratio task (n=6-9 for control, n=7 for mPFC-LH hM4Di, two-way ANOVA). **L** Schematic illustrating the experimental timeline for the progressive ratio in the novel environment and home cage, performed after first progressive ratio task following a washout period. Mice were tested in the dark phase in both home cage and novel cage and were counterbalanced to the order of treatment. See methods for further details. **M** Inhibition of mPFC-LH projecting neurons had no effect on breakpoint reached after a short progressive ratio task in the home cage (dashed lines, n=7 for control, n=6 for mPFC-LH hM4Di, two-way ANOVA), but did significantly increase the breakpoint reached in the novel cage from 4 to 4.5 minutes (solid lines, n=7 for control, n=6 for mPFC-LH hM4Di, two-way ANOVA, p=0.0053) and resulted in a significant group-by-time interaction (p=0.0097). **N** Mice were placed in a novel environment with access to a familiar palatable food 30 minutes following CNO injection (n=10 for control, n=8 for mPFC-LH hM4Di, two-tailed unpaired t-test). **O** Inhibition of mPFC-LH projecting neurons significantly increased intake of the familiar palatable food compared to control (p=0.0457). **P** Latency to approach the familiar palatable was significantly reduced in the mPFC-LH hM4Di group (p=0.0439). **Q** Number of eating bouts were not significantly different between mPFC-LH hM4Di and control groups. **R** mPFC-LH hM4Di mice spent significantly more time eating than controls (p=0.0379), however time sniffing, approaching or time outside of the food zone did not vary between groups. **S** Mice were placed in a familiar environment with access to a novel palatable food 30 minutes following CNO injection (n=10 for control, n=8 for mPFC-LH hM4Di, two-tailed

unpaired t-test). **T** Inhibition of mPFC-LH projecting neurons significantly increased intake of the novel palatable food compared to control (p=0.0477). **U** Latency to approach the novel palatable food was not significantly different between mPFC-LH hM4Di and control groups **V** Number of eating bouts was significantly increased with inhibition of mPFC-LH projecting neurons (p=0.0142). **W** mPFC-LH hM4Di mice spent significantly more time eating than controls (p=0.0197) and significantly less time outside of the food zone (p=0.0173), however time sniffing or approaching food zone did not vary between groups. **W** mPFC-LH hM4Di mice spent significantly more time eating than controls (p=0.0197) and significantly less time outside of the food zone (p=0.0173), however time sniffing or approaching food zone did not vary between groups. All data are mean +/- SEM. For statistical analysis, a indicates a significant main effect of group, b indicates a significant interaction, *p<0.05 and **p<0.01 for between group comparisons. CNO, clozapine-N-Oxide; FED3, feeding experimentation device version 3; LH, lateral hypothalamus; mPFC, medial pre-frontal cortex; ns, not significant.

Figure 5. Chronic ablation of the mPFC-LH increases body weight gain and consumption of novel palatable food. A Schematic illustrating viral strategy for chronic caspase mediated ablation of the mPFC-LH circuit. **B** Caspase injection reduces % area of immunoreactivity of the neuronal marker NeuN in the mPFC (n=13 for control, n=9 for mPFC-LH caspase, two-tailed unpaired t-test, p=0.0241). **C** There was a main effect of mPFC-LH circuit ablation on body weight gain following surgery on a chow diet (n=13 for control, n=12 for mPFC-LH caspase, two-way ANOVA with Sidak's multiple comparison test, p=0.0331) and a significant group-by-time interaction (p=0.0157). Body weight gain in mPFC-LH ablated mice was significantly higher at 3 weeks (p=0.0398) and 13 weeks following surgery (p=0.0231). Orange arrows indicate where mice were transferred to a different room or feeding cages or underwent fasting for feeding or behavior experiments. **D** There was no significant difference in chow intake over a short-term recording period in the feeding cages (n=12 for control, n=10 for mPFC-LH caspase, 1-2 24 hour periods per animal, two-way ANOVA). **E** There was also no significant difference in chow intake following an overnight fast (n=12 for controls, n=12 for mPFC-LH caspase, two-way ANOVA). **F** During a short-term exposure to novel high fat/high sugar diet (HFD) in the feeding cages mPFC-LH caspase mice consumed significantly more HFD per day than controls (n=12 for controls, n=8 for mPFC-LH caspase, two-tailed unpaired t-test, p=0.033). **G** Intake was still significantly higher in the mPFC-LH caspase group when differences in body weight were considered (n=12 for controls, n=8 for mPFC-LH caspase, two-tailed unpaired t-test, p=0.0366). **H** There was a main effect of mPFC-LH circuit ablation on cumulative novel HFD intake (n=12 for control, n=8 for mPFC-LH circuit, 3 24 hour periods per animal, two-way ANOVA with Sidak's multiple comparison test, p=0.0042) and a significant group-by-time interaction (p<0.0001). mPFC-LH circuit ablation resulting in significantly higher HFD intake at 9pm (p=0.012) and from 1am to 6am (p<0.05). All data are mean +/- SEM. For statistical analysis a indicates a significant main effect of group, b indicates a significant interaction, *p<0.05 for between group comparisons. BW, body weight; HFD, high fat/high sugar diet LH, lateral hypothalamus; mPFC, medial pre-frontal cortex.

Figure S1. Injection sites and behavioural data for mPFC-LH hM3Dq mice. A Schematic illustrating spread of retrograde AAV-cre injected into the LH (n=9, darker blue indicates overlapping injection sites between animals). **B** Schematic illustrating spread of hM3Dq-mCherry DREADDs injected into the mPFC (n=9, darker pink indicates overlapping injection sites between animals). **C-H** Mice were placed in the elevated zero maze, light-dark box and open field 30 minutes after intraperitoneal injection (i.p.) of CNO (1mg/kg) (n=11-12 for control,

n=9 for mPFC-LH hM3Dq). mPFC-LH circuit activation had no effect on: **C-D** time in the open arms of the elevated zero maze, entries into the open arms; **E-F** time in the light side of the light-dark box or entries into the light zone; or **G-H** distance travelled and velocity in the open field. All data are mean +/- SEM. CNO, clozapine-N-Oxide; LH, lateral hypothalamus; mPFC, medial prefrontal cortex.

Figure S2. Wireless optogenetic activation of mPFC^{Vglut1}-LH projecting neurons suppresses feeding and promotes avoidance. A Schematic showing viral strategy and probe used for optogenetic activation of the vesicular glutamate transporter-1 (Vglut1) neurons of the mPFC that project to the LH (mPFC^{Vglut1}-LH). Vglut1-cre mice and wild-type (WT) littermates were injected bilaterally into the LH with a retrograde virus encoding for the excitatory opsin hChR2(H134R)-mCherry. A wireless probe with a light emitting diode was inserted into the mPFC. **B** Representative coronal section showing expression of hChR2(H134R)-mCherry (red), with DAPI staining (blue), throughout the mPFC following bilateral injection of retrograde pAAV(rg)-EF1a-double floxed-hChR2(H134R)-mCherry-WPRE-HGHpA into the LH of a Vglut1-cre expressing mouse. CPu, caudate putamen; fmi, forceps minor of the corpus callosum, IL, Infralimbic cortex; and PrL, Prelimbic cortex. **C** Schematic illustrating experimental timeline for fasting re-feeding with photostimulation. **D** Photostimulation of the mPFC^{Vglut1}-LH projecting neurons suppresses re-feeding following an overnight fast (n=7 for WT, n=15 for mPFC^{Vglut1}-LH, two-way ANOVA with Sidak's multiple comparison test). There was a significant main effect of photostimulation on chow intake (WT > mPFC^{Vglut1}-LH, p=0.0287) and a significant group-by-time interaction (p=0.0118), and significantly reduced chow intake in the mPFC^{Vglut1}-LH group compared to WT at 2 hours (p=0.0224) and 4 hours (0.0157). **E** Schematic illustrating the real-time place preference (RTPP) test. Mice were given 10 minutes to explore the RTPP arena before one side of the area was paired with photostimulation for 20 minutes. **F** Representative heat maps from WT (left) and mPFC^{Vglut1}-LH (right) animals during the 20 minute RTPP test. **G** mPFC^{Vglut1}-LH animals reduced their preference for the photostimulation paired side of the RTPP arena (% change from baseline period preference) compared to WT group during the 20 minute RTPP test (n=5 WT, n=12 mPFC^{Vglut1}-LH, two-tailed unpaired t-test, p=0.011). **H** Velocity in the RTPP arena did not change significantly between baseline (no-stim) to the 20 minute RTPP test (stim). **I** Schematic illustrating the progressive ratio task using FED3 during photostimulation and no stimulation. Mice were counterbalanced to the order of treatment and trained on FED3 between progressive ratio test days. See methods for further details. **J** Breakpoint ratio was significantly reduced in the mPFC^{Vglut1}-LH mice under photostimulation conditions compared to no stimulation (n=6 for WT, n=13 for mPFC^{Vglut1}-LH, two-way ANOVA with Sidak's multiple comparison test, mPFC^{Vglut1}-LH No Stim> mPFC^{Vglut1}-LH Stim, p=0.0056), and there was a significant group-by-time interaction (p=0.0169). All data are mean +/- SEM. For statistical analysis, a indicates a significant main effect of group, b indicates a significant interaction, *p<0.05, **p<0.01 for between group comparisons. FED3, feeding experimentation device version 3; LH, lateral hypothalamus; mPFC, medial pre-frontal cortex.

S3 mPFC-LH circuit activity during mild stress or consumption in fed and fasted conditions. A Schematic illustrating spread of retrograde AAV-cre injected into the LH (n=6, darker green indicates overlapping injection sites between animals). **B** Schematic illustrating spread of GCamp7s injected into the mPFC and cannula placement (n=6, darker green indicates overlapping injection sites between animals, dashed boxes indicate cannula position) **C** A subset of mice from the hand in cage experiment in figure 3 E-H were picked up by the tail (n= 3 mice, 3-4 trials per animal, 10 trials in total). mPFC-LH projecting neuron

activity increased prior to coming into contact with researchers hand (time=0). **D** Heatmap showing individual trials of response to contact with hand in order of trial. **E** mPFC-LH projecting neuron activity varied from early entry into a novel environment (entry 2, orange) to final entry (entry 10-20, blue) (n=6 mice, data from figure 3M-P). **F** Peak z-score was significantly lower on the final entry to the novel environment compared to entry 2 (two-tailed paired t-test, p=0.0252). **G** mPFC-LH activity during entry into object zone of a familiar object (n=4 mice, 2-6 zone entries, blue) and a novel object (red) during recording from mPFC-LH projecting neurons. **H** Average z-score following entry into the familiar object zone did not differ significantly from baseline at -5-0s before entry or 0-5s and 5-10s following entry. **I** Average z-score was significantly higher -5-0s prior to entry into the novel object zone than baseline (one-way ANOVA with Dunnet's multiple comparison test, -5-0>-10 -5s, p=0.0171). **J** Heatmap of individual trials into the familiar and novel object zones in order of trial. **K** Food intake during the 2 minute exposure to chow (orange), familiar palatable food (purple), and novel palatable food (pink) shown in figure 3Q-AB (n=3 mice, average over 2-10 trials). Mice ate significantly more familiar palatable food and significantly more novel palatable food compared to chow (one-way ANOVA with Tukey's multiple comparison test; familiar novel food>chow, p=0.0339; novel palatable food>chow, p=0.0423). **L-O** Comparison of average z-scores during consumption of chow, familiar palatable food, novel palatable food and wooden dowel. **N** Average z-score 5-10s following consumption was significantly lower for novel palatable food than for wooden dowel (one-way ANOVA with Tukey's multiple comparison test, wooden dowel> novel palatable food, p=0.191). **O** Average z-score 10-15s after consumption was significantly lower for novel palatable food compared to wooden dowel (one-way ANOVA with Dunnet's, wooden dowel>novel palatable food, p=0.0497). **P-S** mPFC-LH projection neuron activity following pick up of either chow, familiar palatable food, novel palatable food or wooden dowel. **T-S** mPFC-LH projecting neuron activity following consumption of chow, familiar palatable food, novel palatable food or wooden dowel following a short fast. **X** Food intake of chow (orange), familiar palatable food (familiar PF, purple) and novel palatable food (novel PF, pink) over a 2 minute exposure period following a short-term fast (n=3 mice, average of 1-4 trials per animal). Food intake of novel palatable food was significantly greater compared to chow (one-way ANOVA with Tukey's multiple comparison test, novel palatable food>chow, p=0.0447) FP, Familiar palatable, NP, novel palatable. **Y-AB** Average z-score at 5-10s post consumption was not significantly different in a fed (data from figure 3U-W) or fasted state for chow (n=3 mice, 1-4 trials chow, 2-5 trials familiar palatable food, 1-3 trials novel palatable food, and 2-5 trials wooden dowel). All data are mean +/- SEM. Dots (**K** & **X)** represent individual animals, circles (**F**, **H-I**, **L-O**, **Y-AB**) represent individual trials. Dashed lines at 0 (**C**, **E**, **G**, **P-W**) and solid vertical lines at 0 (**D** & **J**) indicate time at which stimulus was delivered or described event occurred. *p<0.05. LH, lateral hypothalamus; mPFC, medial pre-frontal cortex.

Figure S4. Injection sites and behavioural data for mPFC-LH hM4Di mice. A Schematic illustrating spread of retrograde AAV-cre injected into the LH (n=7, darker blue indicates overlapping injection sites between animals). **B** Schematic illustrating spread of hM4Di-mCherry DREADDs injected into the mPFC (n=7, darker pink indicates overlapping injection sites between animals). **C-H** Mice were placed in the elevated zero maze, light-dark box and open field 30 minutes after intraperitoneal injection (i.p.) of CNO (3mg/kg) (n=5-7 for control, n=6-7 for mPFC-LH hMD4i). mPFC-LH circuit inhibition had no effect on: **C-D** time in the open arms of the elevated zero maze, entries into the open arms; **E-F** time in the light side of the

light-dark box or entries into the light zone; or **G-H** distance travelled and velocity in the open field All data are mean +/- SEM. LH, lateral hypothalamus; mPFC, medial prefrontal cortex.

Figure S5. Behavioural data for mPFC-LH Caspase. A-C Mice were placed in the elevated zero maze and open field (n=12-13 for control, n=9-12 for mPFC-LH Caspase). Circuit ablation had no effect on: **A** time in the open arms of the elevated zero maze; **B** distance travelled in the open field; or **C** velocity in the open field. All data are mean +/- SEM. LH, lateral hypothalamus; mPFC, medial prefrontal cortex.

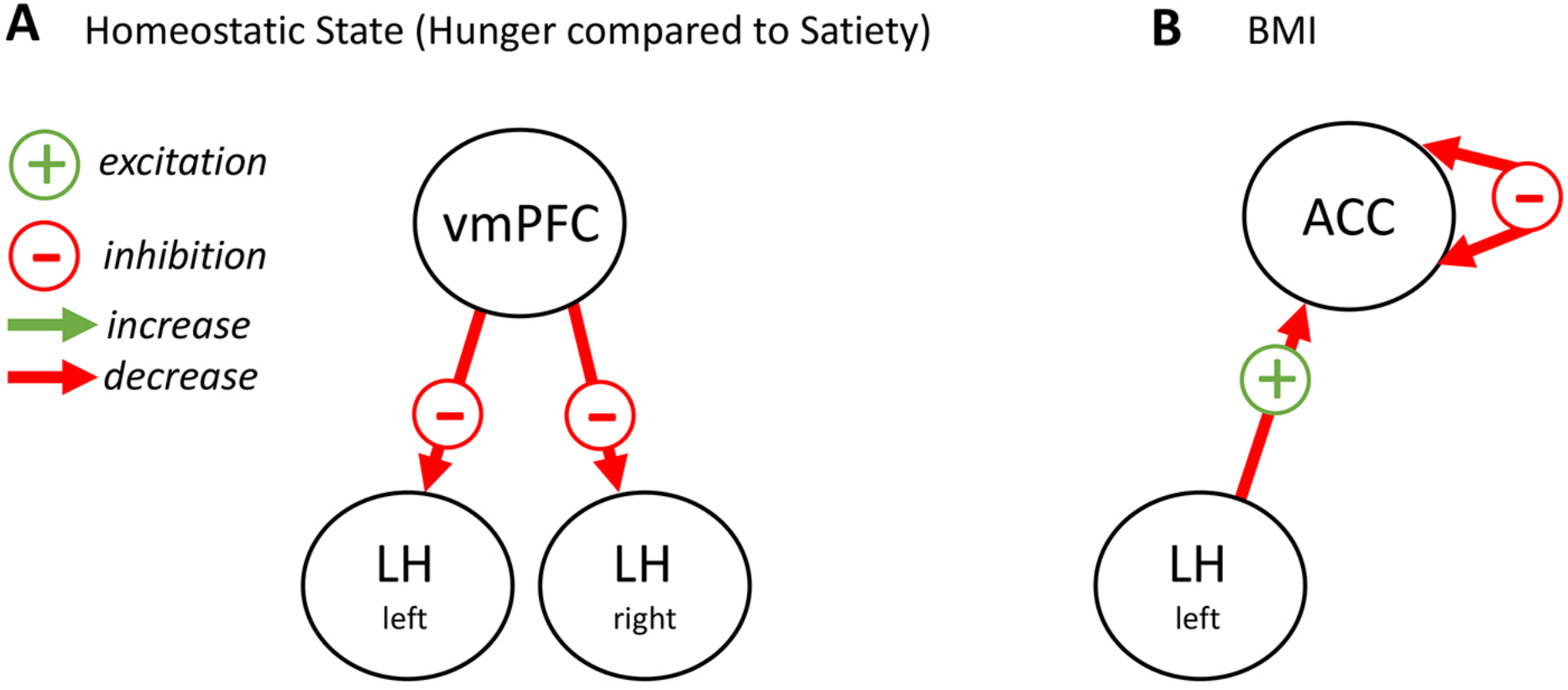
A
Homeostatic State (Hunger compared to Satiety)
excitation
inhibition
increase
decrease
vmPFC
LH
left
LH
right
B
BMI
ACC
LH
left

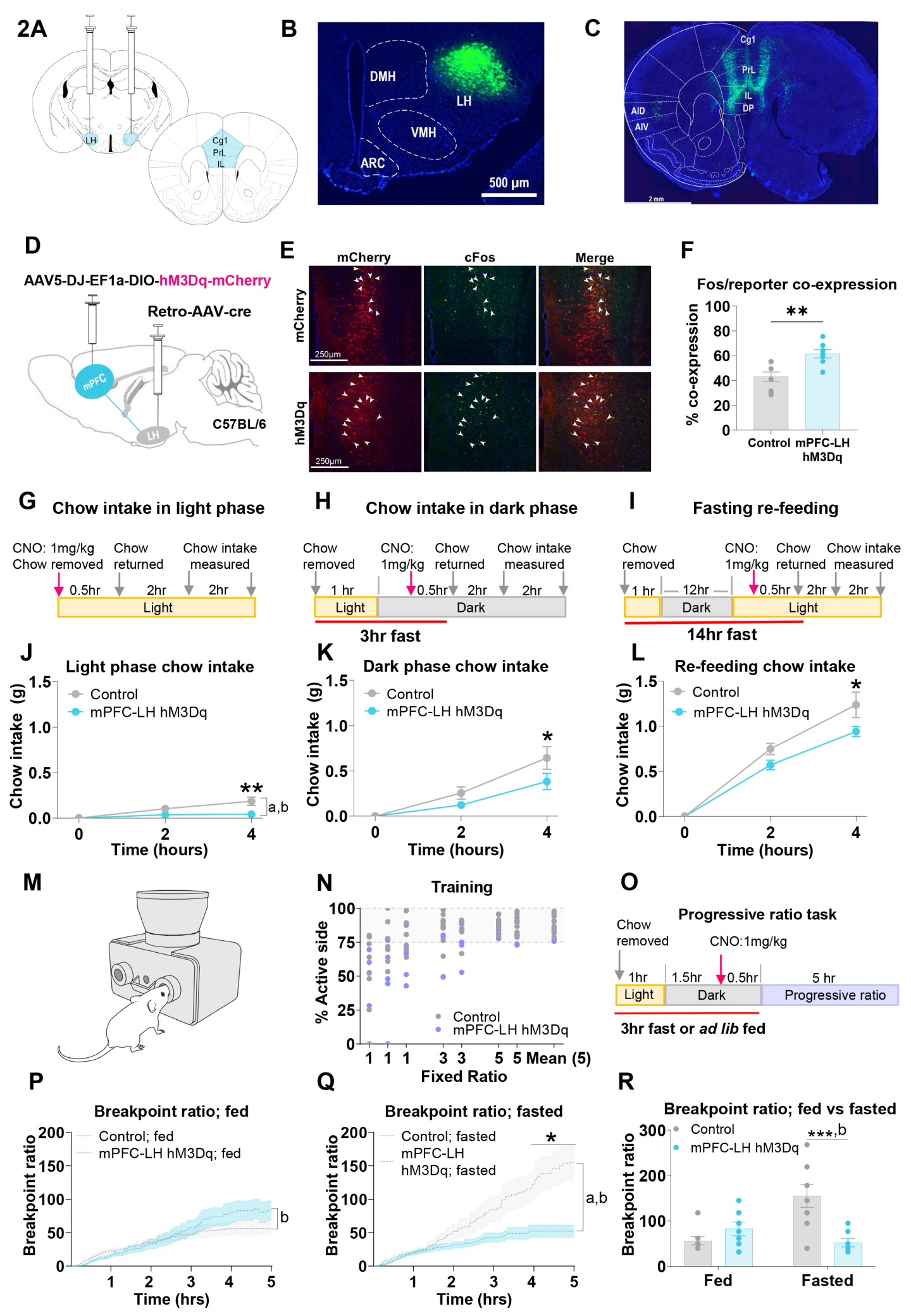
2A
LH
Cg1
PrL
IL
B
DMH
LH
VMH
ARC
500 µm
C
Cg1
PrL
IL
DP
AID
AIV
2 mm
D
AAV5-DJ-EF1a-DIO-hM3Dq-mCherry
Retro-AAV-cre
mPFC
LH
C57BL/6
E
mCherry
cFos
Merge
mCherry
hM3Dq
250µm
F
Fos/reporter co-expression
% co-expression
Control
mPFC-LH hM3Dq
G
Chow intake in light phase
CNO: 1mg/kg
Chow removed
Chow returned
Chow intake measured
0.5hr
2hr
2hr
Light
H
Chow intake in dark phase
Chow removed
CNO: 1mg/kg
Chow returned
Chow intake measured
1 hr
0.5hr
2hr
2hr
Light
Dark
3hr fast
I
Fasting re-feeding
Chow removed
CNO: 1mg/kg
Chow returned
Chow intake measured
1 hr
12hr
0.5hr
2hr
2hr
Dark
Light
14hr fast
J
Light phase chow intake
Chow intake (g)
Control
mPFC-LH hM3Dq
a,b
Time (hours)
K
Dark phase chow intake
Chow intake (g)
Control
mPFC-LH hM3Dq
Time (hours)
L
Re-feeding chow intake
Chow intake (g)
Control
mPFC-LH hM3Dq
Time (hours)
M
N
Training
% Active side
Control
mPFC-LH hM3Dq
Fixed Ratio
O
Progressive ratio task
Chow removed
CNO:1mg/kg
1hr
1.5hr
0.5hr
5 hr
Light
Dark
Progressive ratio
3hr fast or ad lib fed
P
Breakpoint ratio; fed
Breakpoint ratio
Control; fed
mPFC-LH hM3Dq; fed
b
Time (hrs)
Q
Breakpoint ratio; fasted
Breakpoint ratio
Control; fasted
mPFC-LH hM3Dq; fasted
a,b
Time (hrs)
R
Breakpoint ratio; fed vs fasted
Breakpoint ratio
Control
mPFC-LH hM3Dq
***,b
Fed
Fasted

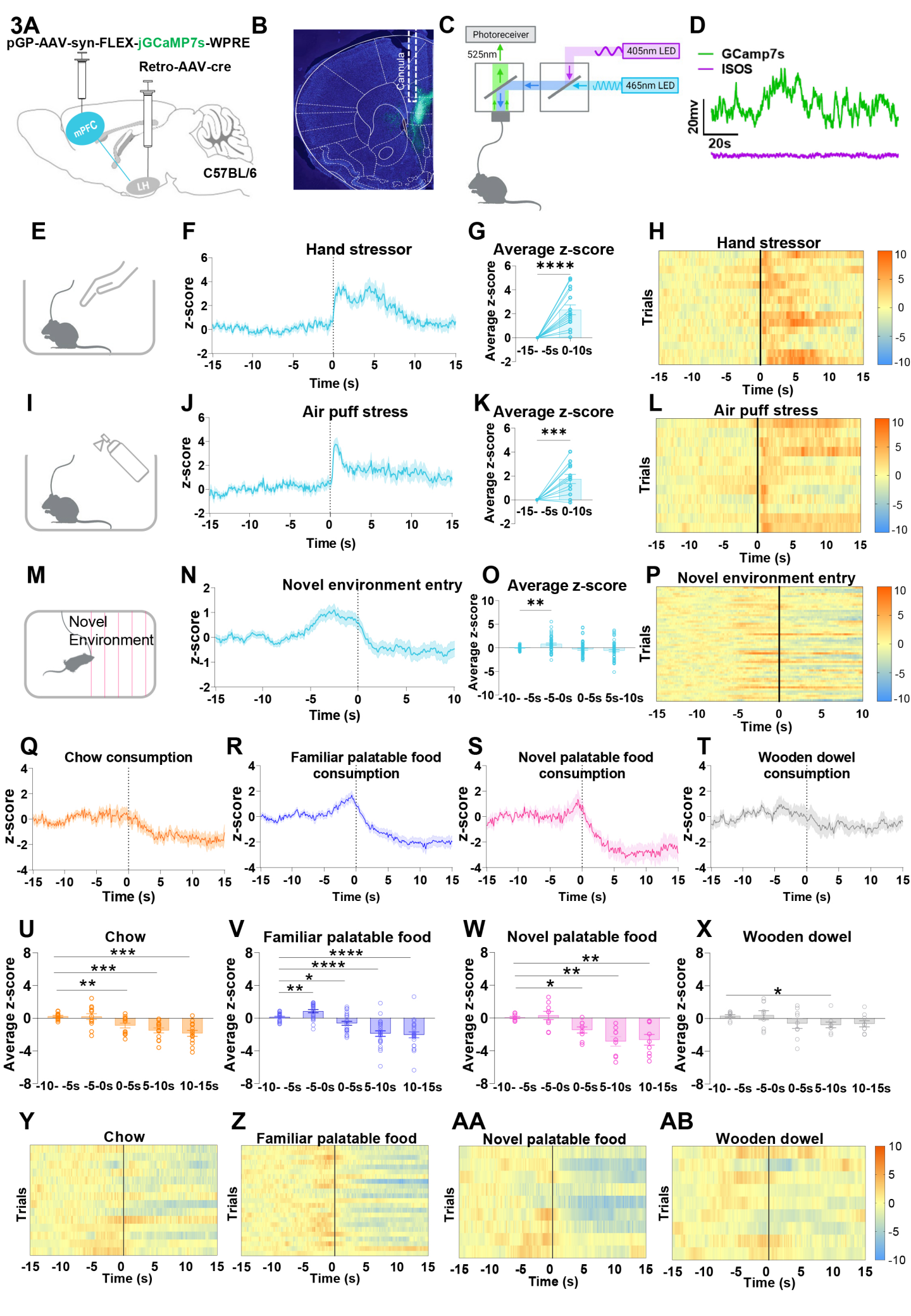
3A
pGP-AAV-syn-FLEX-jGCaMP7s-WPRE
Retro-AAV-cre
mPFC
LH
C57BL/6
B
Cannula
C
Photoreceiver
525nm
405nm LED
465nm LED
D
GCamp7s
ISOS
20mv
20s
E
F
Hand stressor
z-score
Time (s)
G
Average z-score
****
-15- -5s 0-10s
H
Hand stressor
Trials
Time (s)
I
J
Air puff stress
K
Average z-score
***
L
Air puff stress
M
Novel
Environment
N
Novel environment entry
O
Average z-score
**
-10- -5s -5-0s 0-5s 5-10s
P
Novel environment entry
Q
Chow consumption
R
Familiar palatable food consumption
S
Novel palatable food consumption
T
Wooden dowel consumption
U
Chow
V
Familiar palatable food
W
Novel palatable food
X
Wooden dowel
-10- -5s -5-0s 0-5s 5-10s 10-15s
Y
Chow
Z
Familiar palatable food
AA
Novel palatable food
AB
Wooden dowel

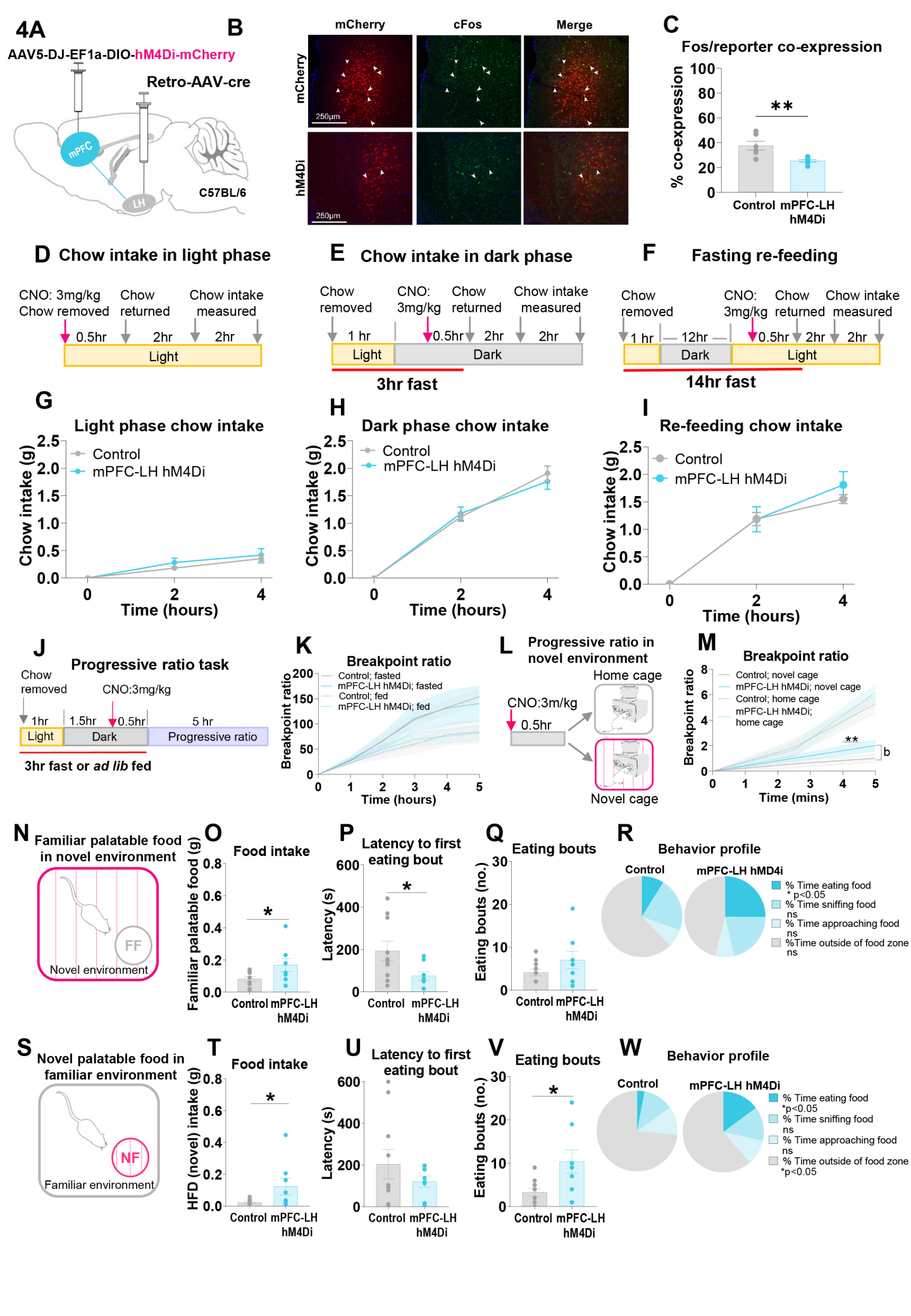
4A
AAV5-DJ-EF1a-DIO-hM4Di-mCherry
Retro-AAV-cre
mPFC
LH
C57BL/6
B
mCherry
cFos
Merge
mCherry
hM4Di
250μm
250μm
C
Fos/reporter co-expression
% co-expression
100
80
60
40
20
0
**
Control
mPFC-LH hM4Di
D Chow intake in light phase
CNO: 3mg/kg
Chow removed
Chow returned
Chow intake measured
0.5hr
2hr
2hr
Light
E Chow intake in dark phase
Chow removed
CNO: 3mg/kg
Chow returned
Chow intake measured
1 hr
0.5hr
2hr
2hr
Light
Dark
3hr fast
F Fasting re-feeding
Chow removed
CNO: 3mg/kg
Chow returned
Chow intake measured
1 hr
12hr
0.5hr
2hr
2hr
Dark
Light
14hr fast
G
Light phase chow intake
Chow intake (g)
Control
mPFC-LH hM4Di
Time (hours)
H
Dark phase chow intake
Chow intake (g)
Control
mPFC-LH hM4Di
Time (hours)
I
Re-feeding chow intake
Chow intake (g)
Control
mPFC-LH hM4Di
Time (hours)
J
Progressive ratio task
Chow removed
CNO:3mg/kg
1hr
1.5hr
0.5hr
5 hr
Light
Dark
Progressive ratio
3hr fast or ad lib fed
K
Breakpoint ratio
Breakpoint ratio
Control; fasted
mPFC-LH hM4Di; fasted
Control; fed
mPFC-LH hM4Di; fed
Time (hours)
L
Progressive ratio in novel environment
CNO:3m/kg
0.5hr
Home cage
Novel cage
M
Breakpoint ratio
Breakpoint ratio
Control; novel cage
mPFC-LH hM4Di; novel cage
Control; home cage
mPFC-LH hM4Di; home cage
**
b
Time (mins)
N
Familiar palatable food in novel environment
FF
Novel environment
O
Food intake
Familiar palatable food (g)
*
Control
mPFC-LH hM4Di
P
Latency to first eating bout
Latency (s)
*
Control
mPFC-LH hM4Di
Q
Eating bouts
Eating bouts (no.)
Control
mPFC-LH hM4Di
R
Behavior profile
Control
mPFC-LH hMD4i
% Time eating food
*p<0.05
% Time sniffing food
ns
% Time approaching food
ns
%Time outside of food zone
ns
S
Novel palatable food in familiar environment
NF
Familiar environment
T
Food intake
HFD (novel) intake (g)
*
Control
mPFC-LH hM4Di
U
Latency to first eating bout
Latency (s)
Control
mPFC-LH hM4Di
V
Eating bouts
Eating bouts (no.)
*
Control
mPFC-LH hM4Di
W
Behavior profile
Control
mPFC-LH hM4Di
% Time eating food
*p<0.05
% Time sniffing food
ns
% Time approaching food
ns
% Time outside of food zone
*p<0.05

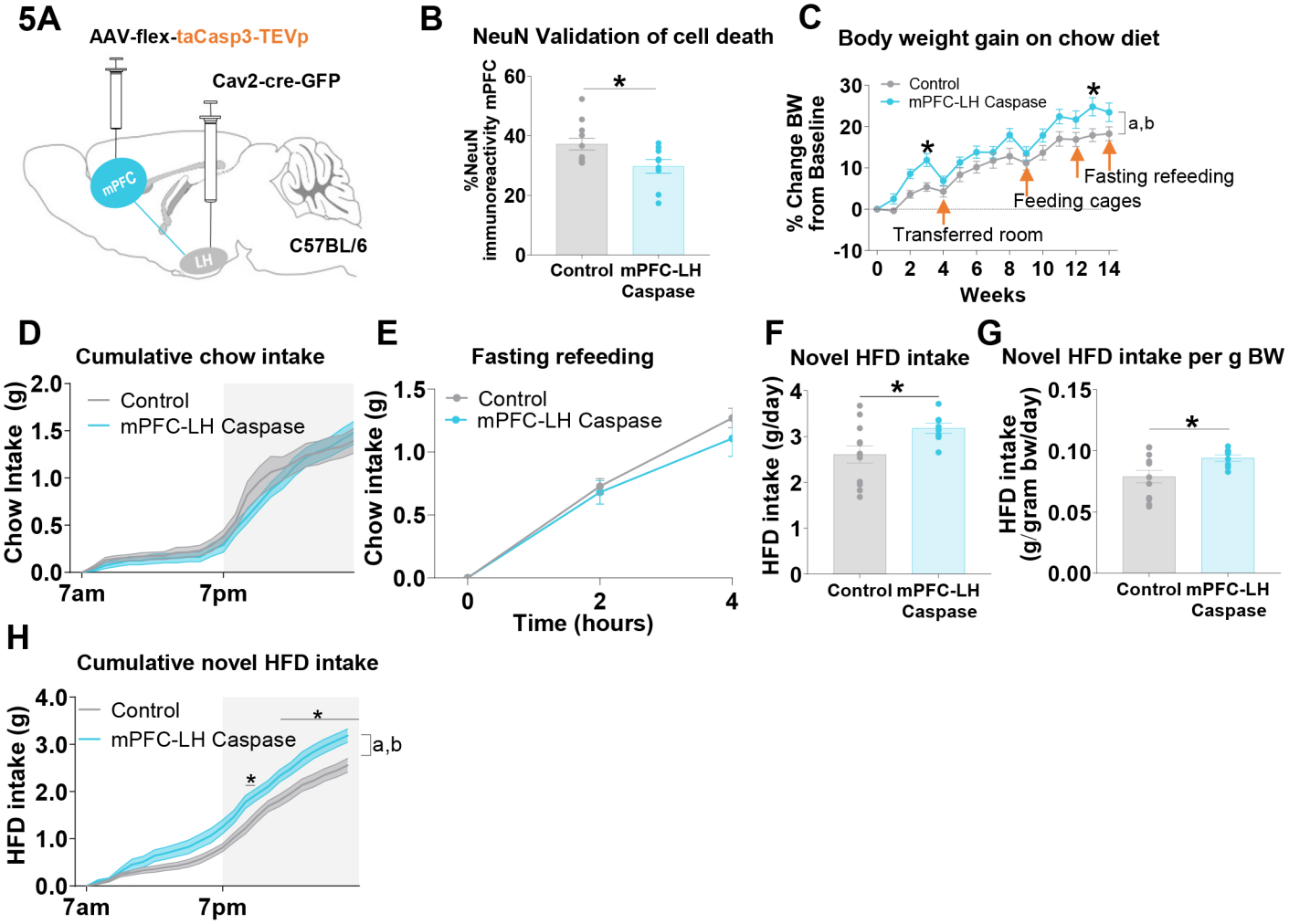
5A
AAV-flex-taCasp3-TEVp
Cav2-cre-GFP
mPFC
LH
C57BL/6
B
NeuN Validation of cell death
%NeuN immunoreactivity mPFC
60
40
20
0
*
Control
mPFC-LH Caspase
C
Body weight gain on chow diet
% Change BW from Baseline
30
20
10
0
-10
Control
mPFC-LH Caspase
*
*
a,b
Fasting refeeding
Feeding cages
Transferred room
0 2 4 6 8 10 12 14
Weeks
D
Cumulative chow intake
Chow Intake (g)
2.0
1.5
1.0
0.5
0.0
Control
mPFC-LH Caspase
7am
7pm
E
Fasting refeeding
Chow intake (g)
1.5
1.0
0.5
0.0
Control
mPFC-LH Caspase
0
2
4
Time (hours)
F
Novel HFD intake
HFD intake (g/day)
4
3
2
1
0
*
Control
mPFC-LH Caspase
G
Novel HFD intake per g BW
HFD intake (g/gram bw/day)
0.15
0.10
0.05
0.00
*
Control
mPFC-LH Caspase
H
Cumulative novel HFD intake
HFD intake (g)
4.0
3.0
2.0
1.0
0.0
Control
mPFC-LH Caspase
*
*
a,b
7am
7pm

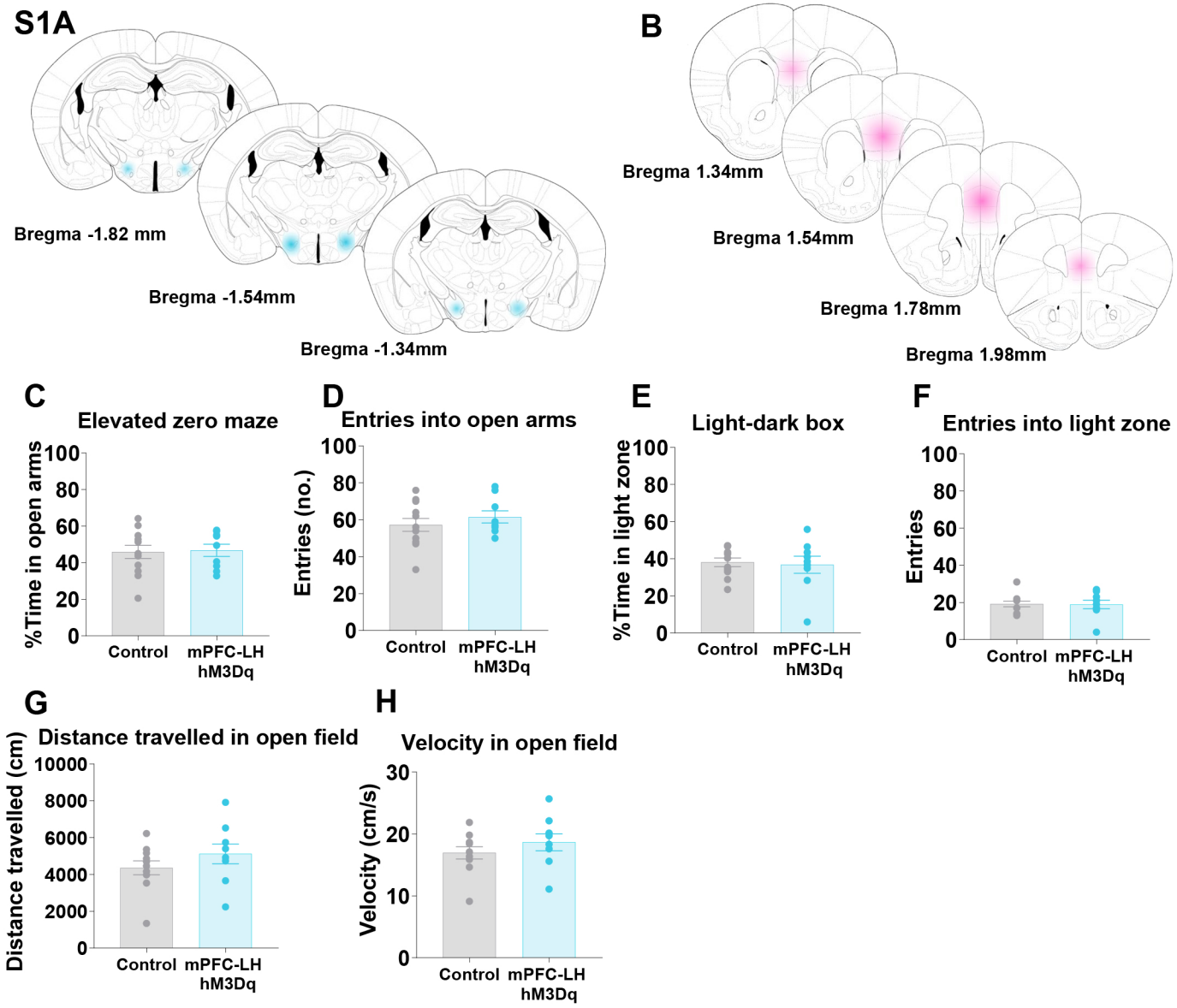
S1A
Bregma -1.82 mm
Bregma -1.54mm
Bregma -1.34mm
B
Bregma 1.34mm
Bregma 1.54mm
Bregma 1.78mm
Bregma 1.98mm
C
Elevated zero maze
%Time in open arms
D
Entries into open arms
Entries (no.)
E
Light-dark box
%Time in light zone
F
Entries into light zone
Entries
G
Distance travelled in open field
Distance travelled (cm)
H
Velocity in open field
Velocity (cm/s)
Control
mPFC-LH hM3Dq

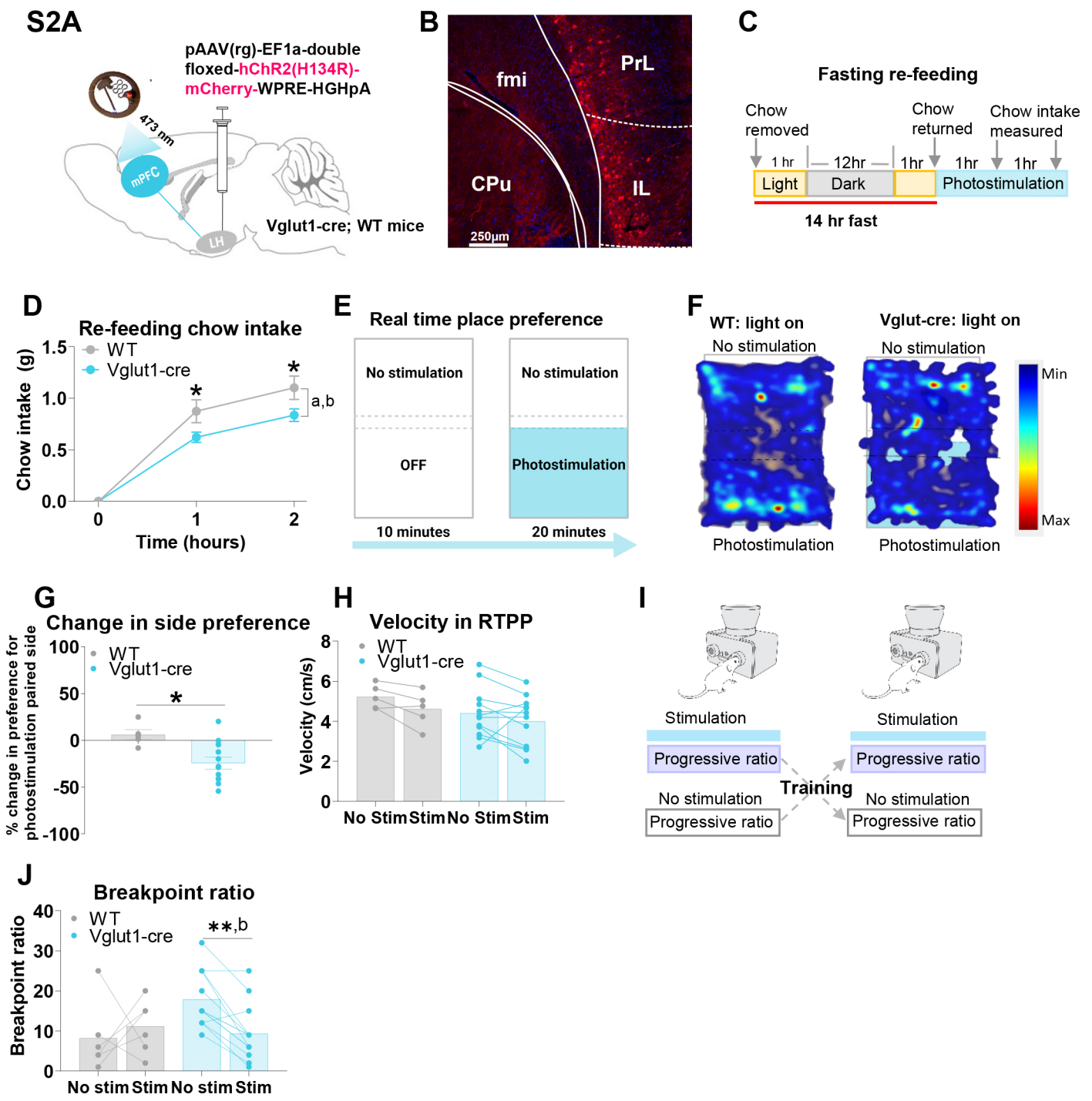
S2A
pAAV(rg)-EF1a-double floxed-hChR2(H134R)-mCherry-WPRE-HGHpA
473 nm
mPFC
LH
Vglut1-cre; WT mice
B
fmi
PrL
CPu
IL
250µm
C
Fasting re-feeding
Chow removed
Chow returned
Chow intake measured
1 hr
12hr
1hr
1hr
1hr
Light
Dark
Photostimulation
14 hr fast
D
Re-feeding chow intake
WT
Vglut1-cre
Chow intake (g)
Time (hours)
a,b
E
Real time place preference
No stimulation
OFF
No stimulation
Photostimulation
10 minutes
20 minutes
F
WT: light on
Vglut-cre: light on
No stimulation
No stimulation
Min
Max
Photostimulation
Photostimulation
G
Change in side preference
WT
Vglut1-cre
% change in preference for photostimulation paired side
H
Velocity in RTPP
WT
Vglut1-cre
Velocity (cm/s)
No Stim
Stim
No Stim
Stim
I
Stimulation
Stimulation
Progressive ratio
Progressive ratio
Training
No stimulation
Progressive ratio
No stimulation
Progressive ratio
J
Breakpoint ratio
WT
Vglut1-cre
Breakpoint ratio
**,b
No stim
Stim
No stim
Stim

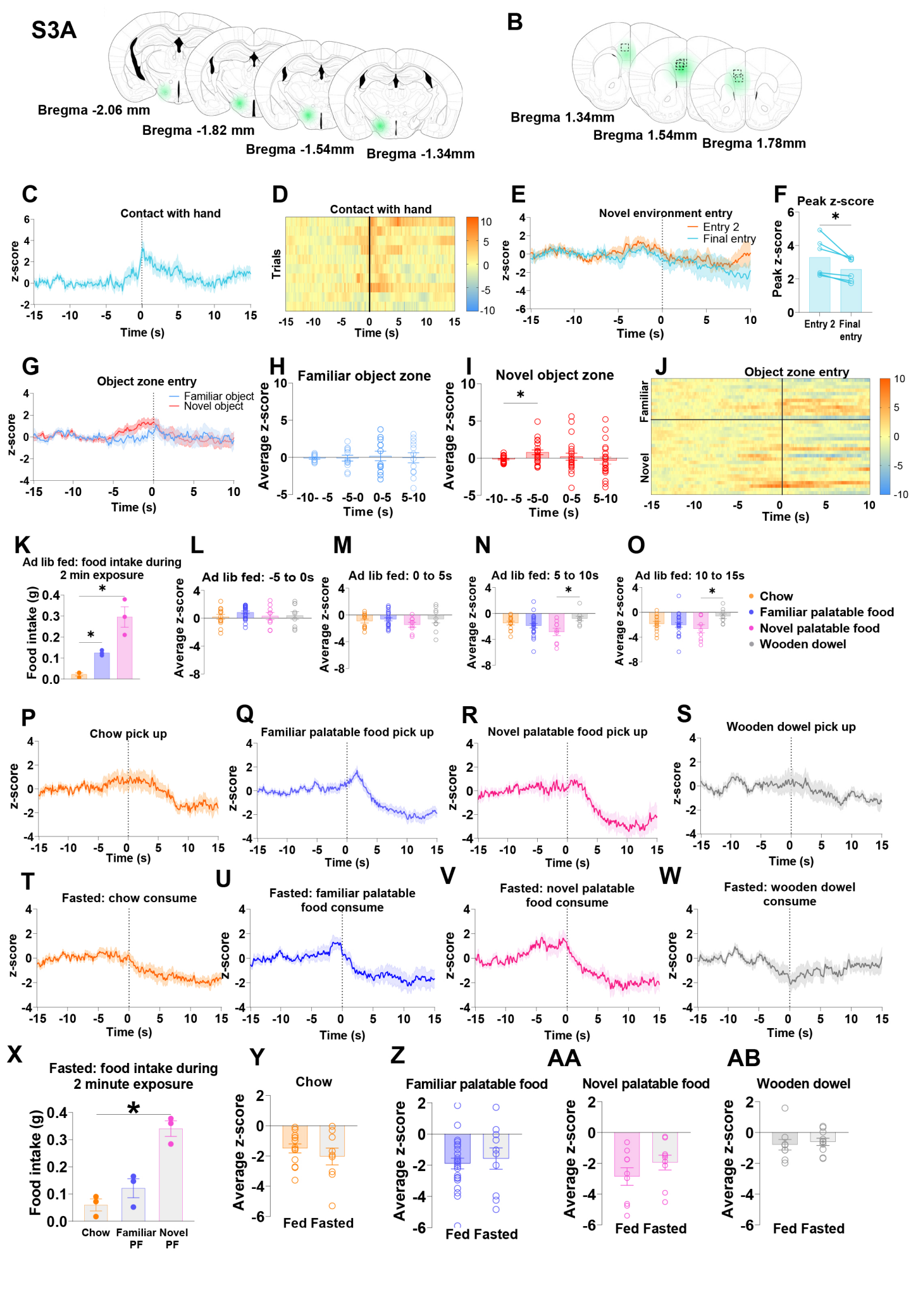
S3A
Bregma -2.06 mm
Bregma -1.82 mm
Bregma -1.54mm
Bregma -1.34mm
B
Bregma 1.34mm
Bregma 1.54mm
Bregma 1.78mm
C
Contact with hand
z-score
Time (s)
D
Contact with hand
Trials
Time (s)
E
Novel environment entry
Entry 2
Final entry
z-score
Time (s)
F
Peak z-score
Peak z-score
Entry 2
Final entry
G
Object zone entry
Familiar object
Novel object
z-score
Time (s)
H
Familiar object zone
Average z-score
Time (s)
I
Novel object zone
Average z-score
Time (s)
J
Object zone entry
Familiar
Novel
Time (s)
K
Ad lib fed: food intake during 2 min exposure
Food intake (g)
L
Ad lib fed: -5 to 0s
Average z-score
M
Ad lib fed: 0 to 5s
Average z-score
N
Ad lib fed: 5 to 10s
Average z-score
O
Ad lib fed: 10 to 15s
Average z-score
Chow
Familiar palatable food
Novel palatable food
Wooden dowel
P
Chow pick up
z-score
Time (s)
Q
Familiar palatable food pick up
z-score
Time (s)
R
Novel palatable food pick up
z-score
Time (s)
S
Wooden dowel pick up
z-score
Time (s)
T
Fasted: chow consume
z-score
Time (s)
U
Fasted: familiar palatable food consume
z-score
Time (s)
V
Fasted: novel palatable food consume
z-score
Time (s)
W
Fasted: wooden dowel consume
z-score
Time (s)
X
Fasted: food intake during 2 minute exposure
Food intake (g)
Chow
Familiar PF
Novel PF
Y
Chow
Average z-score
Fed
Fasted
Z
Familiar palatable food
Average z-score
Fed
Fasted
AA
Novel palatable food
Average z-score
Fed
Fasted
AB
Wooden dowel
Average z-score
Fed
Fasted

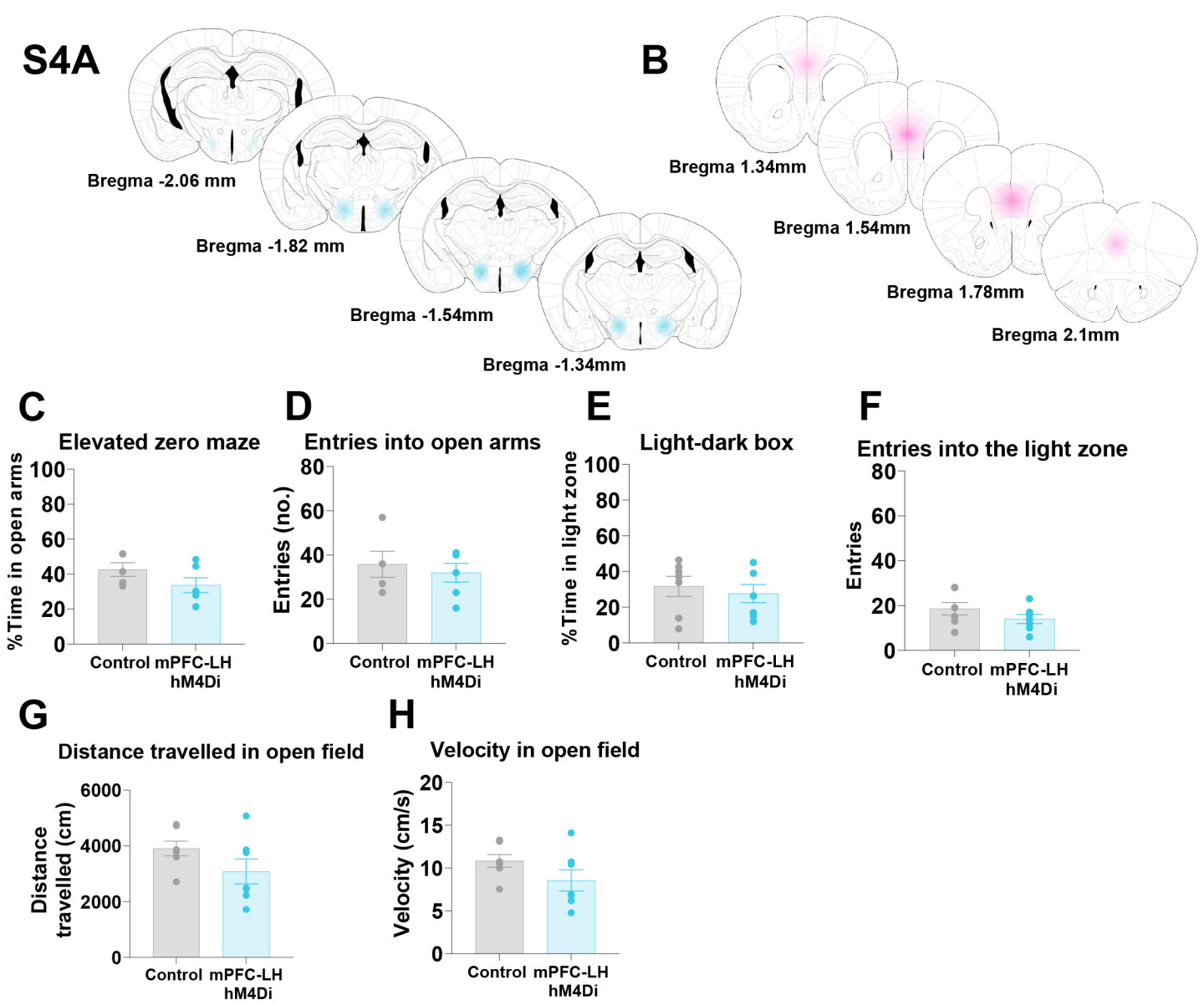
S4A
Bregma -2.06 mm
Bregma -1.82 mm
Bregma -1.54mm
Bregma -1.34mm
B
Bregma 1.34mm
Bregma 1.54mm
Bregma 1.78mm
Bregma 2.1mm
C
Elevated zero maze
% Time in open arms
100
80
60
40
20
0
Control
mPFC-LH hM4Di
D
Entries into open arms
Entries (no.)
80
60
40
20
0
Control
mPFC-LH hM4Di
E
Light-dark box
% Time in light zone
100
80
60
40
20
0
Control
mPFC-LH hM4Di
F
Entries into the light zone
Entries
80
60
40
20
0
Control
mPFC-LH hM4Di
G
Distance travelled in open field
Distance travelled (cm)
6000
4000
2000
0
Control
mPFC-LH hM4Di
H
Velocity in open field
Velocity (cm/s)
20
15
10
5
0
Control
mPFC-LH hM4Di

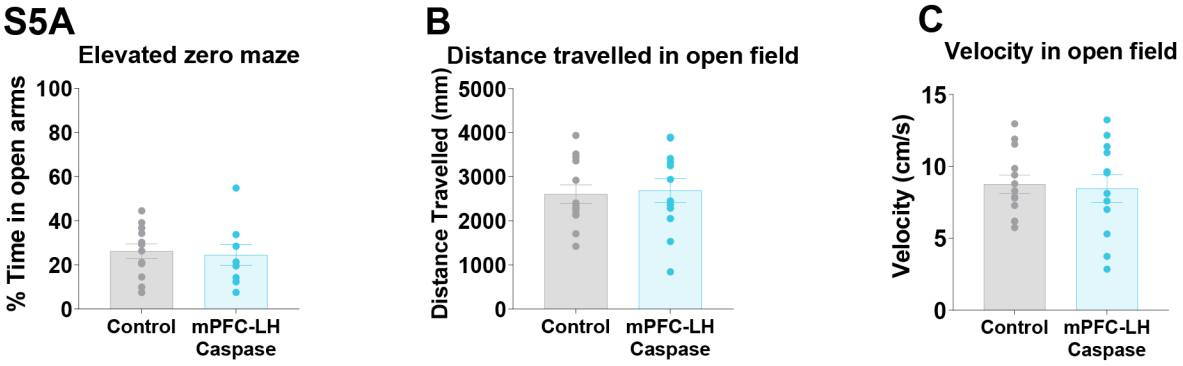
S5A
Elevated zero maze
% Time in open arms
100
80
60
40
20
0
Control
mPFC-LH Caspase
B
Distance travelled in open field
Distance Travelled (mm)
5000
4000
3000
2000
1000
0
Control
mPFC-LH Caspase
C
Velocity in open field
Velocity (cm/s)
15
10
5
0
Control
mPFC-LH Caspase